Uncertainty Assessment in Deep Learning-based Plant Trait Retrievals from Hyperspectral data

Eya Cherif[1,2], Teja Kattenborn[5,3], Luke A. Brown[6], Michael Ewald[7], Katja Berger[8], Phuong D. Dao[9,10,11],

5 Tobias B. Hank[12], Etienne Laliberté[13], Bing Lu[14], Hannes Feilhauer[1,2,3,4]

[1] Institute for Earth system Science and Remote Sensing, Leipzig University, Leipzig, 04103, Germany
[2] Center for scalable data analytics and artificial intelligence (ScaDS.AI), Leipzig University, 04105, Leipzig, Germany
[3] German Centre for Integrative Biodiversity Research (iDiv), Halle-Jena-Leipzig, Germany
[4] Helmholtz-Centre for Environmental Research (UFZ), 04318, Leipzig, Germany
10 [5] Sensor-based Geoinformatics (geosense), University of Freiburg, 79116, Freiburg, Germany
[6] School of Science, Engineering & Environment, University of Salford, Manchester, M5 4WT, UK
[7] Institute of Geography and Geoecology, Karlsruhe Institute of Technology (KIT), 76131 Karlsruhe, Germany
[8] GFZ Helmholtz Centre for Geosciences, Potsdam, 14473, Germany
[9] Department of Agricultural Biology, Colorado State University, Fort Collins, CO 80523, USA
15 [10] Graduate Degree Program in Ecology, Colorado State University, Fort Collins, CO 80523, USA
[11] School of Global Environmental Sustainability, Colorado State University, Fort Collins, CO 80523, USA
[12] Department of Geography, Faculty of Geosciences, Ludwig-Maximilians-Universität München (LMU), 80333, Munich, Germany
[13] Département de Sciences Biologiques et Institut de Recherche en Biologie Végétale, Université de Montréal, Montréal,
20 H1X 2B2, Canada
[14] Department of Geography, Simon Fraser University, Burnaby, BC V5A 1S6, Canada

Correspondence to: Eya Cherif (eya.cherif@informatik.uni-leipzig.de)

Abstract

25 The large-scale mapping of plant biophysical and biochemical traits is essential for ecological and environmental applications. Given its finer spectral resolution and unprecedented data availability, hyperspectral data has emerged as a promising, non-destructive tool for accurately retrieving these traits. Machine and particularly deep learning models have shown strong potential in retrieving plant traits from hyperspectral data. However, when deploying these methods at large scales, reliably quantifying associated uncertainty remains a critical challenge, especially when models encounter out-of-

30 domain (OOD) data, such as unseen geographic regions, species, biomes, or data acquisition modalities. Traditional uncertainty quantification methods for deep learning models, including deep ensembles (Ens_UN) and Monte Carlo dropout (MCdrop_UN), rely on the variance of predictions but often fail to capture uncertainty in OOD scenarios, leading to overoptimistic and potentially misleading uncertainty estimates. To address this limitation, we propose a distance-based uncertainty estimation method (Dis_UN) that quantifies prediction uncertainty by measuring dissimilarity in the predictor

35 and embedding space between training and test data. Dis_UN leverages residuals as a proxy for uncertainty and employs dissimilarity indices in data manifolds to estimate worst-case errors via 95-quantile regression. We evaluate Dis_UN on a

pre-trained deep learning model for prediction of multiple plant traits from hyperspectral images, analyzing its performance across OOD data, such as pixels containing spectral variation from urban surfaces, bare ground, water, clouds or open surface waters. For this study we target six leaf and canopy traits: Leaf mass per area (LMA), Chlorophyll (Chl), Carotenoids (Car), Nitrogen (N) content, Leaf area index (LAI) and Equivalent water thickness (EWT). Results indicate that Dis_UN effectively differentiates between OOD components and provides more reliable uncertainty estimates than traditional methods, which tend to underestimate the range of uncertainty (on average over traits 26.7% for Ens_UN and 6.5% for Dropout_UN). However, challenges remain for traits affected by spectral saturation. These findings highlight the advantages of distance-aware uncertainty quantification methods and underscore the necessity of diverse training datasets to minimize sampling biases and enhance model robustness. The proposed framework improves the reliability of uncertainty estimation in vegetation monitoring and offers a promising approach for broader applications.

1 Introduction

Plant functional traits, including structural, biochemical, physiological, and phenological properties, are fundamental to understanding ecosystem structure, function, and resilience (Lavorel and Garnier, 2002; Reich, 2014; Funk et al., 2017). These traits regulate key ecological processes such as photosynthesis, nutrient cycling, stress response, and productivity (Serbin and Townsend, 2020). The large-scale mapping of plant traits, such as leaf chlorophyll, nitrogen, and water contents, is essential for a range of ecological and environmental applications. These include biodiversity monitoring, Earth system modeling, and vegetation health assessment (Briottet et al., 2022; Cavender-Bares et al., 2020; Houborg et al., 2015; Kissling et al., 2018; Sakschewski et al., 2015; Van Bodegom et al., 2014). However, traditional methods of measuring plant traits via field sampling are resource-intensive, spatially limited, and insufficient to capture global variability. In this respect, hyperspectral data from Earth observation (EO) satellites and airborne sensors have emerged as valuable data sources for predicting functional plant traits (Cavender-Bares et al., 2017; Jetz et al., 2016). These sensors enable the measurement of reflectance across hundreds of narrow and contiguous wavelength bands, which are sensitive to subtle biophysical, biochemical, and structural variations within plant canopies (Jacquemoud and Ustin, 2019). With the recent launch of hyperspectral satellite missions such as Gaofen-5 (GF-5, Ge et al., 2022), Hyperspectral Imaging Satellite (HySIS, Garg et al., 2024), PRecursore IperSpettrale della Missione Applicativa (PRISMA, Cogliati et al., 2021), Environmental Mapping and Analysis Program (EnMAP, Chabrillat et al., 2024), and upcoming Surface Biology and Geology (SBG, Cawse-Nicholson et al., 2021) and Copernicus Hyperspectral Imaging Mission for the Environment (CHIME, Nieke et al., 2023), the volume of hyperspectral data will provide unprecedented opportunities to map plant traits on a global scale and thus advancing ecosystem monitoring (Asner and Martin, 2016; Briottet et al., 2022; Hank et al., 2019).

Machine learning models, particularly deep learning, are highly successful in predicting plant traits from hyperspectral data (Cherif et al., 2023; Pullanagari et al., 2021; Serbin et al., 2019; Singh et al., 2015; Wang et al., 2019, 2020). However, when these models are applied to unseen data, e.g. from different geographical regions, biomes, with unknown scene components (e.g. clouds or shadows), or new sensors—it becomes crucial to assess the uncertainty of the predicted values. This is

particularly important when the predictor space of unseen data deviates from that of the training dataset resulting in out-of-domain (OOD) observations. In addition, the relationship between predictors and the response variable may vary across different geographical regions or biomes due to spatial structures or non-stationarity. While some efforts have been made to quantify uncertainty in the context of hyperspectral plant trait retrieval (García-Soria et al., 2024; Singh et al., 2015; Wang et

75 al., 2019), the results are often not comparable as the definition and interpretability of the uncertainty estimates varies depending on the methods used. Uncertainty quantification is particularly prevalent in EO for vegetation monitoring, where training data is typically sparse, and models are often applied to new, unseen regions and, hence, data that are OOD (Kattenborn et al., 2022; Ploton et al., 2020, Meyer and Pebesma 2021). In addition to providing crucial information on the quality of OOD predictions, quantitative estimates of uncertainty are increasingly utilized in a range of downstream

80 ecological and environmental applications and are often required by data assimilation schemes in order to appropriately weigh all available observations (Chernetskiy et al., 2017; Lewis et al., 2012; Mathieu and O'Niell, 2008). In applications such as the assessment of land surface phenology, for example, recent studies have explored the propagation of plant trait prediction uncertainties to derived phenological metrics (Graf et al., 2023), enabling more robust detection of changes in phenophases (e.g., due to the effects of climate change). The increasing importance of uncertainty estimates is reflected by

85 the recent efforts of space agencies and data providers (Brown et al., 2021b; Gorroño et al., 2018, 2017; Goryl et al., 2023), and uncertainties are now a goal of Analysis Ready Data (ARD) standards (Committee on Earth Observation Satellites, 2024, https://ceos.org/ard/). In addition, recent reports from the European Commission (Camia et al., 2024), highlight uncertainty estimations as a specific quantitative requirement for various European Union land-related environmental and agriculture policies.

90 Uncertainty in model predictions arises from two primary sources: aleatoric uncertainty, which stems from inherent data variability and measurement noise, and epistemic uncertainty, which reflects the model's lack of knowledge or representation related to the modeling choice (García-Soria et al. 2024; Lang et al. 2022; Martínez-Ferrer et al.2022). While aleatoric uncertainty is irreducible as it originates from stochastic measurement errors, epistemic uncertainty can be mitigated by incorporating additional data, refining model complexity, or improving feature representation. Popular methods for

95 estimating epistemic uncertainty, particularly for deep learning models, include bootstrapping (Efron and Tibshirani, 1993), Monte Carlo dropout (Gal and Ghahramani, 2016) and deep ensembles (Lakshminarayanan et al., 2017). These methods rely on the variation in model predictions to estimate uncertainty. For example, with deep ensembles or bootstrapping, the uncertainty is estimated from the variance of predictions obtained from multiple models trained with different subsets of the training data. As they are inherently based on the model training data, the capacity of such approaches to estimate

100 uncertainty in OOD data is limited. For example, multiple predictions on OOD data obtained from an ensemble approach might all be very biased even if the variance is low, which would translate into an underestimation of the uncertainty (Gal et al., 2016). Instead of building on the variance in the predictions, uncertainty estimation for EO should particularly focus on the dissimilarity between the training and the new data. In other words, if an observation is very different from what the model has learned, it is likely to be very uncertain (Meyer and Pebesma, 2021, Linnenbrink et al., 2024). There is, therefore,

105   a need for an uncertainty estimation approach that accounts for dissimilarities between the training and unseen data (Silvan-Cardenas et al., 2008; Khatami et al., 2017; Feilhauer et al., 2021).

To address the challenges of uncertainty quantification, especially in OOD scenarios, distance-based methods have emerged as a promising solution. These methods estimate uncertainty by analyzing the dissimilarity between training and new unseen data. For instance, Janet et al. (2019) proposed a low-cost uncertainty metric for predictions of chemical properties of

110   unknown substances/materials based on the distance of new inputs from the training data in latent space, outperforming traditional uncertainty metrics such as Monte-carlo dropout and ensembles, particularly for data points far from the training set. Meyer and Pebesma (2021) discussed the importance of defining an "area of applicability" for spatial models, emphasizing on the use of dissimilarity metrics to assess model confidence when dealing with new data. Building on this, Papacharalampous et al. (2024) and Linnenbrink et al. (2024) illustrated the effectiveness of distance-based metrics in

115   enhancing uncertainty quantification and improving model reliability in spatial predictions.

In the context of plant trait predictions from hyperspectral data, distance-based uncertainty metrics could offer similar advantages. Hence, this study aims to develop and evaluate a distance-based method for quantifying uncertainty of deep learning models used for plant trait retrievals. Specifically, we propose a distance-based method, hereafter referred to as Dis_UN, to evaluate a previously established multi-trait model when used for inference on OOD data (Cherif et al., 2023).

120   Our approach uses residuals as a proxy for total uncertainty and employs dissimilarity indices in data manifolds to predict the uncertainty. By performing 95-quantile regression, we estimate the upper-bound limit of residuals. Specifically, with an established multi-trait model for trait predictions, we aim to:

      a) assess how effectively this method quantifies uncertainty for OOD vegetation samples at the local scale for six leaf and canopy traits: Leaf mass per area (LMA), Chlorophyll (Chl), Carotenoids (Car), Nitrogen (N) content, Leaf area

125   index (LAI) and Equivalent water thickness (EWT). To achieve this, we iterate over 50 datasets, each time training a multi-trait model that serves as the foundation for generating and evaluating our distance-based uncertainty estimates.

      b) demonstrate the method's potential at the landscape scale with hyperspectral scenes, investigating how the model performs when confronted with OOD observations—such as pixels containing spectral variation from urban surfaces, bare ground, water, clouds or open surface waters.

130

2 Methods

2.1 Distance-aware uncertainty quantification (Dis_UN)

We introduce a distance-based approach to estimate the absolute residuals of a deep learning model (referred to as uncertainty) based on the degree of dissimilarity between training data and new, unseen samples (Fig. 1). We acknowledge

135   that error is not exactly the same as uncertainty in the probabilistic sense but can be a significant contributing component (JCGM, 2008; Widlowski, 2015). However, for the purposes of this analysis, we adopt this definition as we approximate the upper bound of the residuals. To accomplish this, we adopted the 'dissimilarity index' (DI) originally presented by Meyer and Pebesma (2021). Our proposed methodology builds on data splits of a cross-validation obtained from evaluating the deep

learning model. Specifically, we distinguish between two subsets: the training sets, which includes the data used to train the
140   deep learning model, and the test sets, which comprises unseen data (ODD) used for evaluation (Fig. 1). These splits enable
systematic quantification of uncertainty by comparing unseen samples to the training data through several manifolds.
Dis_UN is subsequently modelled using 95-quantile regression with calculated DIs serving as predictors. We applied this
method to hyperspectral imagery to evaluate estimated uncertainties for OOD data. To assess the performance of Dis_UN at
the local-scale on OOD vegetation data, we used a one hold-out set. For landscape-scale OOD data, we assess if the
145   uncertainty is elevated on unseen or unrelated scene components compared to the uncertainty of vegetated areas, such as
clouds, shadows, urban areas, or waterbodies. In this setting, we benchmarked our method against two state-of-the-art
approaches: Monte Carlo dropout (MCdrop_UN) and the deep ensemble (Ens_UN) method.
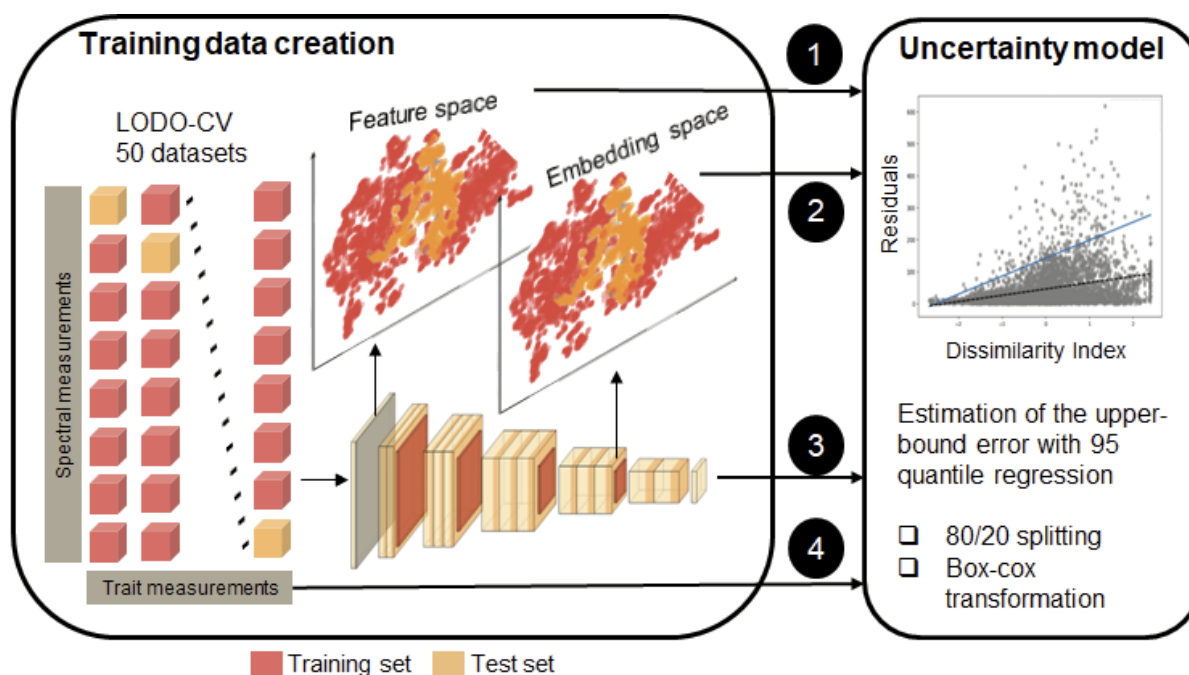
150   **Figure 1: Workflow of the distance-based uncertainty method (Dis_UN) to assess uncertainty of a deep learning model. The
method consists of two phases: Training data generation for uncertainty estimation using leave-one-dataset-out cross-validation
(LODO-CV) on the deep learning model, and uncertainty modeling, which incorporates the following inputs: 1) distance between
the training and the test samples in feature space, 2) distance in the embedding space of the multi-trait model, 3) the trait
predictions obtained from the deep learning models and 4) the true trait observations.**

155

2.1.1 The Multi-trait Model

The deep learning model evaluated in our study builds upon a Convolutional Neural Network (CNN) originally proposed by
Cherif et al. (2023). This model is based on the EfficientNet-B0 architecture with a customization that optimizes the model

for one-dimensional spectral data, making it well-suited for predicting multiple plant traits from hyperspectral reflectance.
160   The structure allows the model to capture both localized spectral features and broader spectral patterns, enabling it to learn
the relationships between spectral signals and plant traits.

The training dataset for this model was extended in this study to 50 compiled datasets (Herrmann et al., 2011; Pottier et al.,
2014; Singh et al., 2015; Hank et al., 2015, 2016; Wang et al., 2016; Wocher et al., 2018; Ewald et al., 2018; Cerasoli et al.,
2018; Ewald et al., 2020; Kattenborn et al., 2019; van Cleemput et al., 2019; Brown, 2019; Chlus et al., 2020; Wang et al.,
165   2020; Burnett et al., 2021; Dao et al., 2021; Rogers et al., 2021; Brown et al., 2021a; Brodrick et al., 2023; Chadwick et al.,
2023; Zheng et al., 2023; Gravel et al., 2024, Table S3), incorporating spectra and trait observations from multiple
ecosystems, including forests, grasslands, shrublands, and agricultural regions. This curation resulted in a sparse dataset with
limited trait observation availability and an imbalanced number of samples across the original datasets. Reflectance data,
spanning wavelengths from 400 to 2500 nm, were gathered from a variety of hyperspectral sensors, including proximal as
170   well as airborne instruments. In line with Cherif et al. 2023, linear interpolation was applied to standardize the diverse
measurements across the full spectral range of 400–2500 nm in 1 nm increments. To address known challenges associated
with atmospheric water absorption in open-sky canopy reflectance spectra, we excluded the water absorption regions (1251–
1529 nm, 1801–2050 nm, and 2451–2501 nm). The remaining three spectral segments were independently smoothed using a
Savitzky-Golay filter (Savitzky and Golay, 1964) with a 65 nm window size. In total, 1522 interpolated spectral bands were
175   retained for analysis. The corresponding trait observations encompassed both biochemical (such as N and pigment contents)
and structural traits (e.g., LMA, LAI), chosen to represent a diverse range of plant functions. For this analysis, we focused on
six leaf and canopy traits: LMA, Chl, Car, N content, LAI, and EWT. This heterogeneous training set was intended to ensure
broader ecological and environmental representativeness, enhancing the model's generalizability. Yet, the collected data do
not provide a fully global representation due to the labor-intensive nature of data collection and the inherent bias in available
180   data measurements (Table S2).

The feature space of the CNN model is constructed from the full spectral range of the reflectance data. This feature space
allows the model to distinguish nuanced spectral differences, effectively mapping them to plant traits. Additionally, an
embedding space is generated from the final convolutional layers of the model, producing a high-dimensional, condensed
representation of the spectral data (Fig. S1). This embedding effectively distills essential spectral patterns while enhancing
185   the model's ability to identify trait relationships.

The model was evaluated using a leave-one-dataset-out cross-validation (LODO-CV), ensuring that each dataset (n = 50)
was held out once as a test set. This cross-validation facilitated an assessment of the model's performance across different
vegetation types and spectral configurations. Using the LODO-CV and the obtained models' residuals of the trait
predictions, training samples were created to estimate uncertainty in the multi-trait model. This dataset included the 1)
190   feature space, that is the hyperspectral data, 2) the embedding space of the multi-trait model, 3) the trait predictions obtained
from the deep learning models and 4) the true trait observations (Fig.1).

2.1.2 Dissimilarity indices (predictors)

The DI, used as a predictor in this study, was calculated using the cosine distance, a well-suited metric for analyzing

195   reflectance data. The cosine distance effectively captures the angular relationship between two spectra (Kruse et al., 1993), emphasizing spectral shape while minimizing the influence of amplitude variations that occur uniformly across the spectrum. This helps mitigate brightness changes caused by heterogeneous illumination and internal shading (Feilhauer et al. 2010).

This DI was applied in both the feature space and the embedding space of the models (Fig. S2). As a first step, we calculated cosine distances between each sample of the test dataset and the samples of the training data set. These calculations were

200   performed using the Python package FAISS (Douze et al., 2024), which is optimized for fast similarity search and clustering of large datasets. As a next step, each DI was calculated as the median of the distance distribution between a test sample and its 50 nearest neighbors in the training set. To ensure comparability across samples, the indices were normalized against the mean DI value of the entire training set (Meyer and Pebesma, 2021).

As reference data for the uncertainty models (Dis_UN), the residuals were used as a proxy for the uncertainty for each trait.

205   This corresponds to the difference between the reference trait data and the trait predictions from the multi-trait models.

The two indices, representing dissimilarities in the feature and the embedding space, and the absolute residuals were then used as input data for the supervised uncertainty estimation (Dis_UN).

2.1.3 Dis_UN Model Training

210   We developed a distinct Dis_UN model for each plant trait, utilizing the DIs calculated for each sample of the test datasets within the LODO-CV as predictors. We partitioned the dataset into training and validation subsets using an 80/20 hold-out split for model performance evaluation. The training of the Dis_UN models was conducted using 95-quantile regression, a statistical technique that allows for the estimation of the 95th percentile of the target distribution (Koenker and Hallock, 2001). This approach is particularly advantageous for uncertainty quantification as it focuses on the upper tail of the error

215   distribution, providing insight into how large the errors can be in the worst-case scenarios (up to 5% of the cases, JCGM 2008). Quantile regression better captures variability because it directly models specific points in the distribution of the target variable, allowing it to represent asymmetries and tail behaviors that mean-based approaches inherently overlook or smooth out. The fit criterion for quantile regression is the pinball loss function, which is specifically designed to penalize deviations from the predicted quantile (Koenker and Hallock, 2001).

220   We addressed potential imbalances in the distribution of the target variable using a histogram-based weighting scheme. We divided the target variable (residuals for each trait) into five bins according to its distribution. Samples in less populated bins, which typically correspond to more extreme or uncommon uncertainty values, were assigned higher weights. These weights were calculated as the inverse of the proportion of samples within each bin, effectively emphasizing the importance of accurately predicting higher levels of uncertainty. This weighting scheme was integral to the training process, as it enhanced

225   the model's sensitivity to the tails of the distribution, where uncertainty is usually highest. Additionally, we applied data transformations on the training data (calculated DIs) as the dissimilarity indices exhibit long-tailed distributions and varying

value ranges (Fig. S2). Specifically, a Box-Cox transformation was applied to the predictor variables followed by a standardization to normalize their distribution and reduce skewness.

2.2 State-of-the-Art Uncertainty Estimation Methods

Monte Carlo Dropout and deep ensembles are considered the gold standard methods for quantifying the epistemic uncertainty (Abdar et al. 2021, Liu et al. 2023). Below, we outline these approaches.

2.2.1 Monte Carlo Dropout for Uncertainty Estimation (MCdrop_UN)

Monte Carlo dropout is a state-of-the-art method that approximates the posterior distribution in Bayesian deep learning (Gal and Ghahramani, 2016). The core concept of MCdrop_UN is to use dropout not only during the training phase, but also during inference, thus enabling the estimation of model uncertainty in a simple, probabilistic manner without requiring significant architectural modifications. Originally, dropout was introduced as a regularization method and is implemented by randomly deactivating a fraction of neurons during training. In MCdrop_UN, this randomness is extended to inference, allowing the creation of an ensemble of predictions without having multiple models.

To quantify uncertainty, multiple forward passes are performed on the input data while keeping dropout active. Each pass generates a different set of neuron activations, effectively simulating different sub-networks. By aggregating these predictions, the mean serves as the final output, while the variability among the predictions (i.e., the standard deviation) reflects the epistemic uncertainty. In our analysis, we calculated the standard deviation of 50 repeated forward passes of the multi-trait model on unseen data with a dropout rate of 0.5 enabled during inference.

2.2.2 Deep Ensembles for Uncertainty Estimation (Ens_UN)

Deep ensembles represent another approach for uncertainty estimation in deep learning (Deng et al., 2022). This method leverages the power of multiple independently trained models to achieve more reliable predictions and uncertainty quantification. The key idea behind deep ensembles is to train several models from scratch, each with random initialization and potentially using different subsets of data, often achieved through bootstrapping. By using different random seeds for weight initialization, each model takes a unique path through the parameter space, ensuring a diverse collection of models. During inference, all the models in the ensemble make predictions for the same input data. The final prediction is calculated by averaging the outputs of all ensemble members, while the variance among these predictions provides an estimate of the epistemic uncertainty. For our analysis, we utilized the mean and standard deviation of the predictions from 50 independently trained models, which were established during the LODO-CV process of the multi-trait model as described in Section 2.1.1.

2.3 Evaluation

2.3.1 Evaluation Using Hyperspectral Imagery (HSI): EnMAP and NEON

To evaluate the different uncertainty estimation methods under extreme OOD conditions, we selected two distinct hyperspectral datasets, each sourced from a different sensor platform: the EnMAP satellite and the National Ecological Observatory Network (NEON) airborne observation platform (AOP), each differing in spatial resolution and environmental context. The first dataset is sourced from the Environmental Mapping and Analysis Program (EnMAP, Chabrillat et al.,

265   2024). The EnMAP mission carries a hyperspectral instrument on a satellite platform and has been designed as a scientific precursor for future more operational spectroscopy missions. EnMAP captures spectral data across the visible, near-infrared (VNIR), and short-wave infrared (SWIR), covering wavelengths from 420 to 2450 nm and comprising 224 spectral bands in total. This dataset offers a spatial resolution of 30 m and a swath width of 30 km, enabling analysis of medium-scale land cover features. The dataset includes a clip of a scene of the city of Leipzig, captured on June 27, 2022 (Fig. 2). This product

270   was downloaded in L2A format (orthorectified and atmospherically corrected, De Los Reyes et al., 2023) from the EnMAP portal (https://planning.enmap.org/). The second dataset comes from NEON's AOP, which provides high spatial and spectral resolution hyperspectral imagery collected annually over various ecological monitoring sites across the United States (Kampe et al., 2010). The NEON AOP spectrometer covers a spectral range from 380 to 2510 nm, resulting in approximately 426 spectral bands with 6 nm spectral sampling (Kampe et al., 2010; Wang et al., 2020). The NEON dataset

275   features a spatial resolution of about 1 m, which allows for the detailed analysis of fine-scale land cover features. This image is a clipped section of a scene at Little Rock Lake (LIRO) from NEON's Great Lakes Domain (D05) captured on August 16th 2020, and processed as a Level 3 (L3): Mosaicked and orthorectified Surface Directional Reflectance (Fig. 2, see details in   data.neonscience.org/api/v0/documents/NEON.DOC.001288vB   and data.neonscience.org/api/v0/documents/NEON.DOC.004365vB). This product was downloaded from the NEON portal

280   (https://data.neonscience.org/data-products/DP3.30006.001). Both datasets include a mix of scene components, such as vegetation, urban areas, water bodies, clouds, and shadows, leading to pixels with mixed signals from different elements. This diversity was intentionally selected to evaluate the robustness of uncertainty estimation methods in detecting OOD samples.
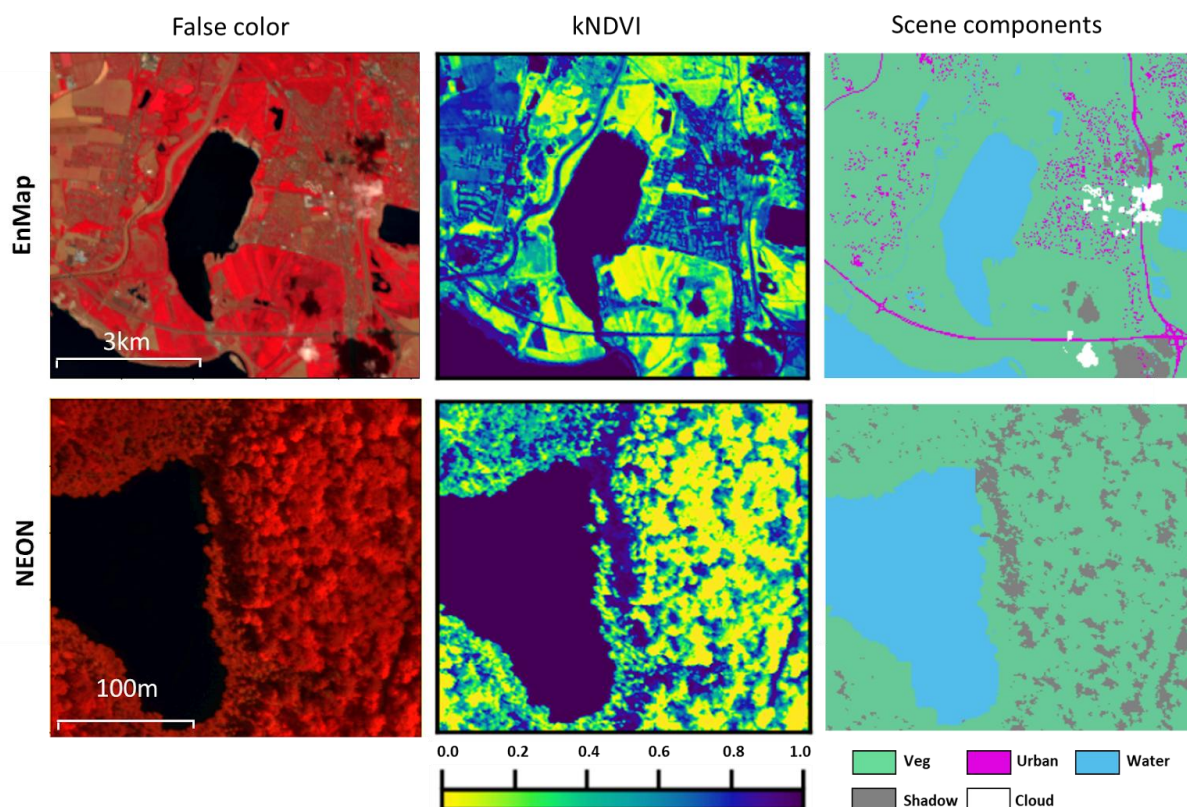
Figure 2: Two study cases for uncertainty inference. Spaceborne scene from EnMAP with 30 m spatial resolution (South of Leipzig, Germany) and an airborne scene from the NEON observatory with 1 m spatial resolution (Little Rock Lake (LIRO) from NEON's Great Lakes Domain (D05), US). In the middle is the kernel normalized difference vegetation index (kNDVI, Camps-Valls et al.; 2021) and on the right side a map of the scene components.

2.3.2 Scene Components' identification

To identify the different components within each scene, we utilized a combination of data sources: OpenStreetMap (OSM: https://download.geofabrik.de/) and manual labeling for certain features, such as clouds, cloud shadows, and tree shadows. The land cover data for urban areas and water bodies were primarily derived from OSM. The maps were resampled to match the spatial resolution of the hyperspectral images. The urban areas included only buildings and highway features. Manual labeling was employed for features like clouds, cloud shadows, and tree shadows. Particularly for tree shadows of the NEON scene, we delineated cloud and tree shadows with a carefully selected threshold of the NIR band (~824 nm). For clouds we used an aggregation band of RED (~650 nm) and BLUE (~444 nm) for delineation. The final scene component maps were generated by integrating the OSM data with the manually labeled elements (Fig. 2).

2.3.3 Uncertainty Evaluation Metrics

To evaluate the performance of our uncertainty estimation methods, we employed different metrics for OOD on local and landscape scale analyses. These metrics quantify how well each model's predicted uncertainties align with actual residuals, as well as the model's ability to identify OOD samples based on elevated uncertainty predictions when compared to vegetated areas. For the local scale OOD analysis, we used the Expected Normalized Calibration Error (ENCE, eq1, Levi et

305 al., 2022; Scalia et al., 2020) as a primary metric to assess how well predicted uncertainties aligned with the actual residuals of the deep learning model predictions. Lower ENCE values signify better model calibration, whereas higher values indicate poorer alignment between predictions and actual residuals, meaning that the model's uncertainty predictions do not accurately reflect the observed errors. The ENCE was computed as Eq. (1):

$$\text{ENCE} = \frac{1}{K}\sum_{i=1}^{K}\frac{|RMSE(b_i)-UE(b_i)|}{UE(b_i)}, \tag{1}$$

310 where K is the total number of bins, $RMSE(b_i)$ is the root mean squared in bin i and $UE(b_i)$ is the uncertainty estimation in bin i.

To evaluate the extent to which the predicted uncertainty range matches the observed range for each trait, we also computed a quantile-based ratio (QuRatio, Eq. (2)). This metric quantifies the proportion of the actual uncertainty range that the model's predictions cover and is calculated as Eq. (2):

315 $$\text{QuRatio}(\%) = \frac{qu95(pred\_UN) - qu5(pred\_UN)}{qu95(obs\_UN) - qu5(obs\_UN)}, \tag{2}$$

where $qu95$ and $qu5$ represent the 95th and 5th quantiles, respectively, of the predicted uncertainty values ($pred\_UN$) and observed uncertainty values (obs_UN).

For the OOD analysis, we aimed to evaluate the model's ability to detect OOD samples by predicting elevated uncertainty values. To quantify this, we used two statistical metrics: the Kolmogorov–Smirnov (K-S) statistical test and the Jeffries-

320 Matusita (JM) distance. These metrics measure the degree of separation between the distributions of predicted uncertainties for different scene components, specifically between vegetated and non-vegetated pixels (Richards et al., 2022; Wacker and Landgrebe, 1972). For each OOD component, we balanced the sample count by sampling to match the least represented component within each category (vegetated and non-vegetated). This approach ensures a fair comparison, as different categories are not equally represented in a scene. We then calculated and compared the distribution of predicted uncertainties

325 across these samples. The JM distance, ranging from 0 to 2, quantifies the separation between distributions, with 0 indicating perfect overlap and 2 representing perfect separation. Higher JM values thus reflect a stronger ability of the model to distinguish OOD samples through uncertainty predictions.

3 Results

330 **3.1 Uncertainty for OOD Vegetation data**

Both the Ens_UN and MCdrop_UN methods demonstrated substantial underestimation of predicted residuals (5th to 95th quantile range) across all traits (Fig. 3). For the Ens_UN method, the predicted uncertainty for LMA covered only 29% of the observed range in residuals. This underestimation was even more pronounced for N, where only 26% was captured, and for Chl and Car, where just 22-25% of the observed range was captured. This pattern highlights a limited ability of Ens_UN

335 to reflect true variability in uncertainty across traits. The ENCE values for Ens_UN varied between 1.4 and 2.2, indicating inconsistent calibration across traits (Table S5).

The MCdrop_UN method exhibited an even greater underestimation of residuals, with predicted uncertainties covering only 5% to 6% of the observed range (Fig. 3), suggesting a particularly narrow predicted interval that does not align well with actual residuals. Correspondingly, MCdrop_UN's ENCE values ranged from 7.8 to 17.6, indicating a substantial

340 misalignment between predicted uncertainties and observed residuals (Table S5).

In contrast, the distance-based method Dis_UN provided a broader and more balanced range of uncertainty estimates. For traits like LMA and N, Dis_UN produced uncertainties that exceeded the observed range of residuals (107.4%, 86.7%; Table S4), indicating a more robust approach of the upper-bound error estimation. For other traits, such as Chl, LAI, EWT, and Car, Dis_UN captured 22.6% to 77.9% of the observed range (Table S4), suggesting that it achieves a more reliable and

345 well-calibrated uncertainty estimate. Dis_UN's ENCE values ranged from 0.44 to 0.53 (Table S5), with data points clustering below the 1:1 line across all traits. This pattern indicates a tendency to overestimate uncertainties, ensuring a conservative uncertainty estimation in which the predicted uncertainties encompass the residuals. Across the different vegetation types represented in the training samples, grassland pixels consistently displayed lower uncertainty values, particularly with Dis_UN, while more heterogeneous vegetation types, such as shrubland and forest, exhibited a broader

350 spread in uncertainty (Fig. 3).

Across different plant traits, we observed different relationships between modelled uncertainty and the spectral and embedding distances, respectively, as indicated by the regression coefficients of the 95-quantile regression. The standardized spectral distance consistently shows higher coefficients compared to embedding space distance across all traits (Table S6). For instance, the spectral distance coefficient for LMA is 53.74, significantly higher than the embedding distance coefficient

355 of 7.07. Similarly, for EWT, the spectral distance coefficient is 4.36, while the embedding distance contributes only 0.86. This trend is also observed across traits like Carotenoid content, where spectral distance (0.81) outweighs embedding distance (0.10). These differences suggest that spectral distance provides a stronger signal in the regression model than the distances in the embedding space.
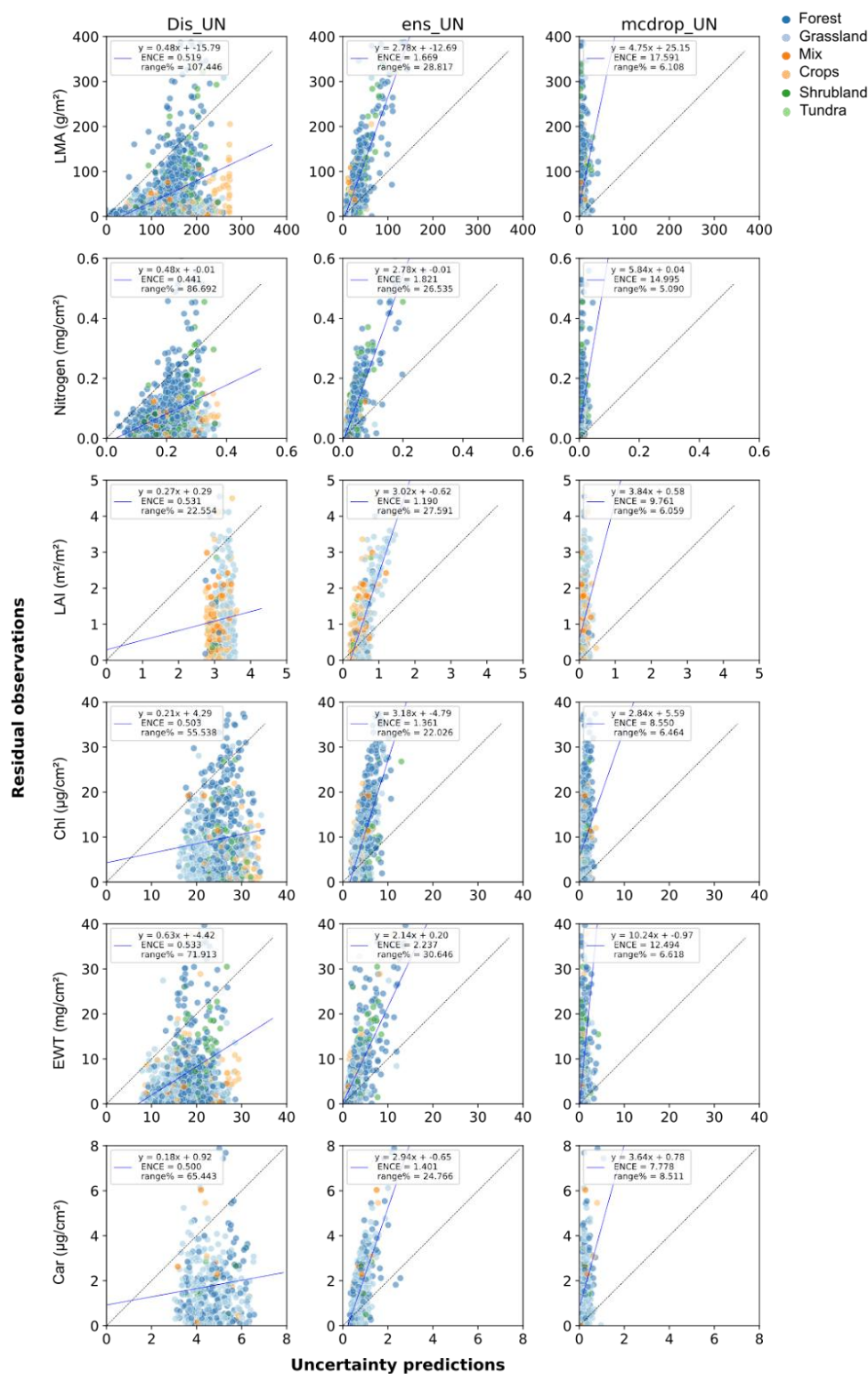
360 **Figure 3: Scatter plots comparing the predicted uncertainties from three methods—distance-based (Dis_UN), ensemble (Ens_UN), and Monte Carlo dropout (MCdrop_UN)—against observed residuals of the multi-trait models across six traits: Leaf Mass per Area (LMA), Nitrogen content, Chlorophyll content (Chl), Equivalent Water Thickness (EWT), Leaf Area Index (LAI), and Carotenoid content (Car). For evaluation we show the Expected Normalized Calibration Error metric (ENCE) and well as the ratio of predicted and observed ranges (Table S5).**

365

3.2 Uncertainty for OOD data

Predicted uncertainty values from the Dis_UN model were consistent across different scene components, with vegetation components showing lower uncertainty and OOD components, such as clouds or water bodies, exhibiting higher uncertainty (Figs. 4 and 5).

370 In the EnMAP scene (Fig. 4), notable spatial variations were observed in the predicted uncertainties from the Dis_UN method across the different traits, particularly for non-vegetative pixels, including shadows, clouds, and waterbodies. These components showed the largest uncertainty, as reflected by their respective JM distances. Uncertainty predictions for traits such as LMA, N and EWT as well as pigments followed similar patterns, with clear differentiation between vegetation and non-vegetation pixels, achieving a higher JM distance of 0.51.

375 Among the traits, LAI showed distinct uncertainty patterns. The coefficient of variations (CV) of the predicted uncertainty values varied between 11.34 and 23.27% for all the traits except for LAI showing a uniform predicted values of CV 4.79%. Despite the low variation, LAI exhibited relatively lower uncertainty for water, shadow and cloud pixels and elevated uncertainties in vegetated areas. Across all traits, uncertainty value distributions from OOD samples (cloud, urban and shadow) were significantly different when compared to vegetated samples (KS test, $p < 0.005$ for all traits).

380 Similar results were obtained for the NEON scene (Fig. 5), with predicted uncertainties consistently lower for vegetation components and higher for OOD scene components like tree shadows and water. The JM distances were higher than those of the EnMAP scene ranging between 0.49 to 0.62 among traits. Tree-covered areas (forest) exhibited greater variance with bimodal distribution, while water pixels had the highest uncertainty levels.

385
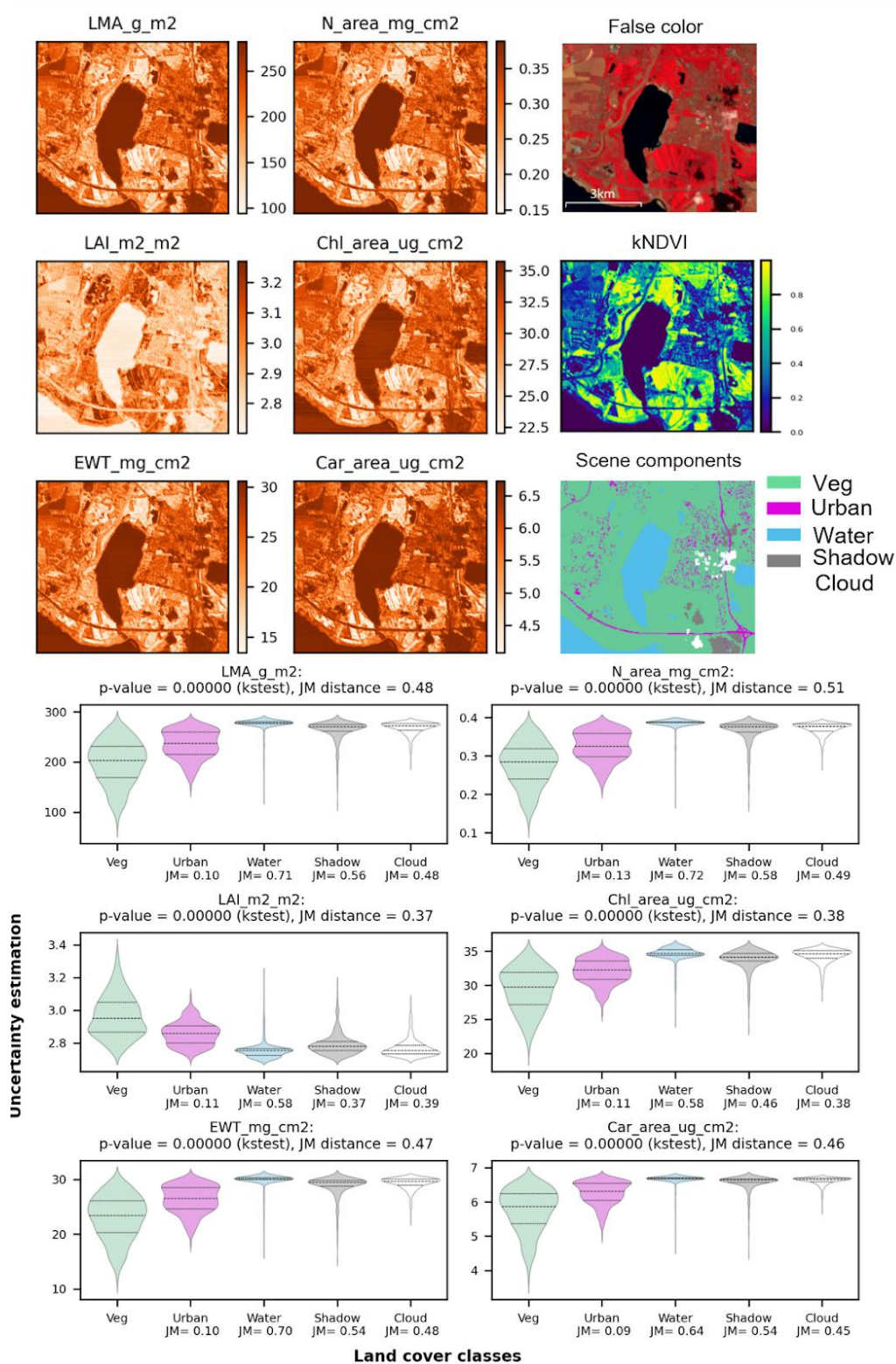
Figure 4: (right panel) Description of the scene: False-color EnMAP scene highlights vegetation in red, kernel normalized difference vegetation index (kNDVI) map shows higher values for denser vegetation area and component scene map. (left panel) Spatial distribution of uncertainty estimation across the EnMAP scene for six plant traits: Leaf Mass per Area (LMA), Nitrogen content (N), Leaf Area Index (LAI), Chlorophyll content (Chl), Equivalent Water Thickness (EWT), and Carotenoid content (Car). (bottom panel) Violin plots of uncertainty estimation for each trait across different scene components, with statistical significance (Kolmogorov–Smirnov p-values) and Jeffries Matusita (JM) distances for class separability: for each plot the JM distance between the vegetated and all non-vegetated data distributions is calculated.

390
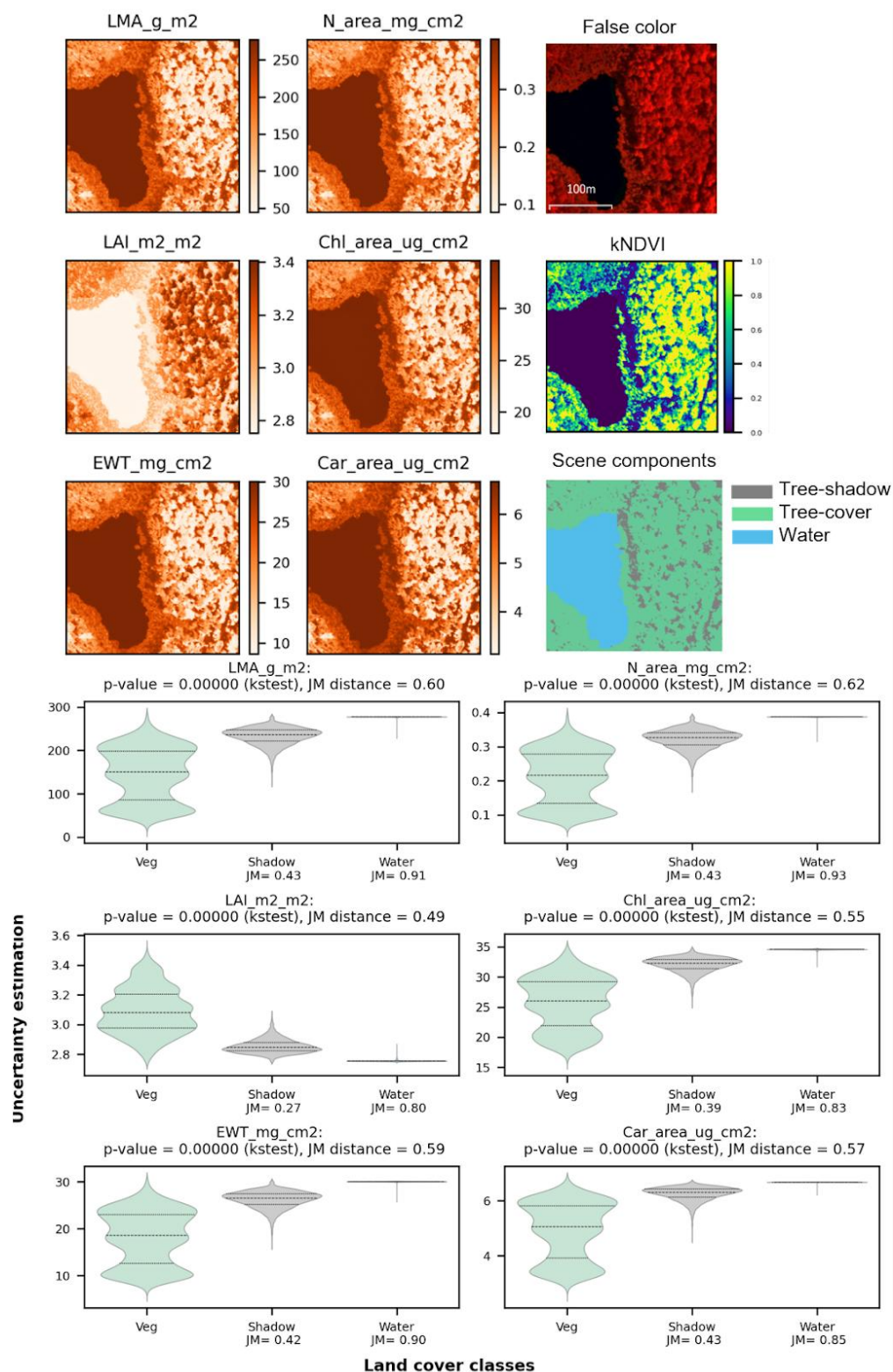
Figure 5: (right panel) Description of the scene: False-color EnMAP scene highlights vegetation in red, kernel normalized
difference vegetation index (kNDVI) map shows higher values for denser vegetation area and component scene map. (left panel)
Spatial distribution of uncertainty estimation across the Neon scene for six plant traits: Leaf Mass per Area (LMA), Nitrogen
content (N), Leaf Area Index (LAI), Chlorophyll content (Chl), Equivalent Water Thickness (EWT), and Carotenoid content
(Car). (bottom panel) Violin plots of uncertainty estimation for each trait across different scene components, with statistical
significance (Kolmogorov–Smirnov p-values) and Jeffries Matusita (JM) distances for class separability: for each plot the JM
distance between the vegetated and all non-vegetated data distributions is calculated.

Consistent with the findings from the OOD vegetation analysis (Section 3.1), MCdrop_UN displayed the lowest
performance in distinguishing between scene components, with the smallest JM distances relative to the vegetation related
uncertainty distribution (Fig. 6 and 7, Fig. S12 and S14). In contrast, the spatial pattern of estimated uncertainties was
generally similar for Ens_UN and Dis_UN, with both methods showing lower uncertainties for vegetation and higher
uncertainties for water and cloud-shadow pixels. However, Dis_UN provided a clearer contrast between non-vegetated and
vegetated pixels.
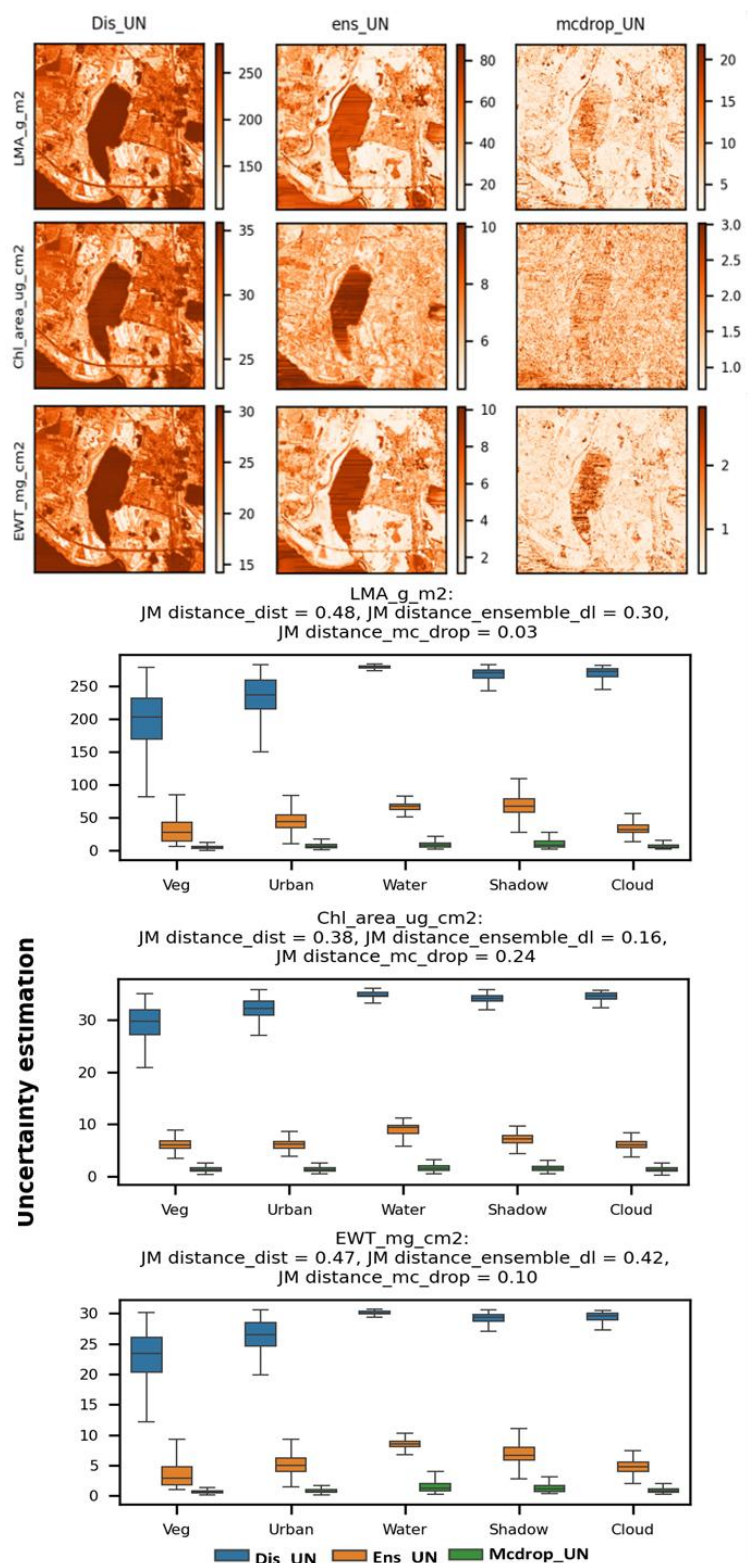
Figure 6: EnMAP scene: Comparison of uncertainty estimations for three traits (Leaf Mass per Area (LMA), Chlorophyll content

410 **(Chl) and Equivalent Water Thickness (EWT)) using three methods: Distance-based (Dis_UN), Ensemble (Ens_UN), and Monte Carlo dropout (MCdrop_UN): (Upper panel): Spatial maps of the uncertainty distribution of LMA, Chl, and EWT for each method. (Bottom panel): Box plots show uncertainty distributions across different scene components (Vegetation, Cloud, Shadow, Urban, Water) for each method. Jeffries Matusita (JM) distances and Kolmogorov-Smirnov (KS) tests quantify the separability of vegetated pixels with non-vegetated classes for all methods.**

415
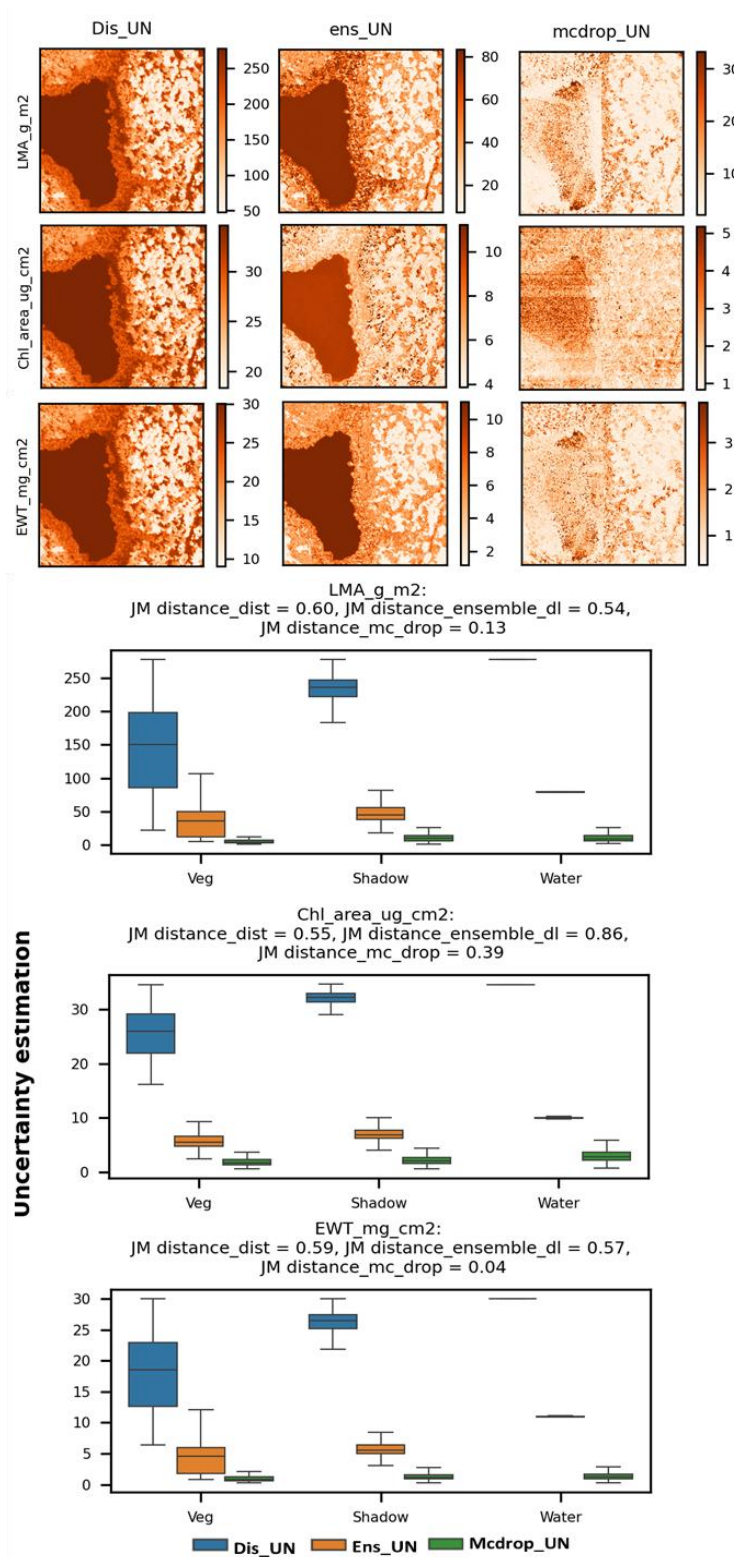
Figure 7: NEON scene: Comparison of uncertainty estimations for three traits (Leaf Mass per Area (LMA), Chlorophyll content (Chl) and Equivalent Water Thickness (EWT)) using three methods: Distance-based (Dis_UN), Ensemble (Ens_UN), and Monte Carlo dropout (MCdrop_UN): (Upper panel): Spatial maps of the uncertainty distribution of LMA, Chl content, and EWT for each method. (Bottom panel): Box plots show uncertainty distributions across different scene components (Vegetation, Cloud, Shadow, Urban, Water) for each method. Jeffries Matusita (JM) distances and Kolmogorov-Smirnov (KS) tests quantify the separability of vegetated pixels with non-vegetated classes for all methods.

4 Discussion

Understanding and accurately quantifying uncertainty is essential for assessing the reliability of model predictions, particularly in OOD scenarios where the model encounters unseen data. In this section, we evaluate the performance of different uncertainty estimation methods at both the local and landscape scales, highlighting their strengths and limitations in capturing uncertainty across various vegetation types and scene components.

4.1 Local-Scale Uncertainty in OOD Vegetation data

In this study, both the Ens_UN and MCdrop_UN methods tended to largely underestimate residuals when applied to OOD vegetation data (on average 26.7% and 6.5% respectively, Table S4 and Fig. S3). The observed low correlation between predicted uncertainty and residuals suggests that the uncertainty estimates produced by these models do not fully represent the model's errors (Fig. 3). This underestimation, especially for higher predicted values, is a known limitation of ensemble and Monte Carlo-based approaches (Hu et al., 2022; Klotz et al., 2022; Lakshminarayanan et al., 2017; Meyer and Pebesma, 2021), which tend to be optimistic in their uncertainty estimates. A similar trend of predicted uncertainty was observed across all traits with both methods (Fig. 3). The Monte Carlo approach, in particular, performed poorly (high ENCE values), indicating its failure to capture variability within samples from different vegetation types.

These findings emphasize the importance of carefully selecting and interpreting uncertainty estimation methods. One key factor to consider is the use of expanded uncertainty, as defined by the Guide to the Expression of Uncertainty in Measurement (Guide to the expression of uncertainty in measurement (GUM), JCGM 2008), which incorporates a coverage factor to ensure a specified confidence level. For instance, we found that the underestimation issue in Ens_UN improved when applying a coverage factor of 2 to approximate a 95% confidence interval (i.e., calculating uncertainty as 2×standard deviation, Fig. S5). However, this adjustment did not improve MCdrop_UN (Fig. S5).

In contrast, the distance-based quantile regression method (Dis_UN) demonstrated a stronger correlation between predicted uncertainty values and the residuals of the multi-trait model but with exaggerated values (Fig. 3, worst-case uncertainty). This indicates that the conservative estimates provided by Dis_UN effectively contain the residuals, a valuable characteristic for uncertainty modeling as highlighted by Brown et al. (2021b). A key advantage of the Dis_UN method is the dissociation of predicted uncertainty values of different vegetation types (Fig. 3), which enhances interpretability. This can be attributed to the incorporation of spectral distance as a predictor (feature space). By leveraging spectral distance, the Dis_UN method

450   quantifies how far a given sample is from typical spectral signatures in the training dataset, allowing for more accurate
adjustment of the predicted uncertainty intervals. The regression analysis supports this observation, highlighting the higher
importance of the scaled spectral distance compared to embedding space distance in predicting residuals across all traits
(Table S6). For instance, the spectral distance coefficients for traits such as LMA, EWT, and Car are significantly higher
than the corresponding coefficients for embedding distance. This indicates that spectral distance contributes more strongly to
455   the regression model's ability to predict uncertainty. The prominence of spectral distance suggests that it is more related to
the diversity in trait values, as it directly reflects the physical and chemical properties captured in the hyperspectral
reflectance data. In contrast, the embedding distance, while useful, abstracts the data into a latent space, which may lose
some trait-specific spectral information. The predicted uncertainty was directly related to the vegetation characteristics. For
example, grassland samples tended to have lower uncertainty across most traits compared to forest and shrubland (Fig. 3).
460   This can be explained by the fact that grassland is one of the more highly represented land cover types in the dataset (1403 of
5573 samples, Table S1) and, from a radiative transfer point of view, it is one of the simpler and homogeneous classes
compared to more complex vegetation types like forests and shrubland (Asner, 1998; Ollinger, 2011; Brown et al., 2024).
Grasslands exhibit less spectral complexity, reducing the likelihood of large residuals. However, forests and shrublands
contain many surface elements beyond green leaves—such as stems, bark, canopy shadow, and other non-photosynthetic
465   components in the background in the gaps between canopies—that contribute to the spectral measurements but are not
directly related to the traits being measured, such as leaf traits. Moreover, the 3D geometry of forests and shrubs can be very
complex. This results in a unique spectral-biophysical relationship in these vegetation types. In contrast, grasslands, with
their predominantly homogeneous structure, show minimal spectral divergence, leading to a reduced uncertainty.

The behavior of uncertainty also varied across different traits, influenced by both the inherent properties of each trait, the
470   trait variability and representativeness of data samples from various vegetation types (e.g., forest, grassland, crops). For
example, the uncertainty modeling for LMA and N showed a better fit to the training data compared to LAI, Chl, and Car
content (Fig. 3 and Fig. S4). This can be attributed to differences in how these traits influence spectral reflectance. LAI is
highly prone to spectral saturation, where the spectral signal becomes less sensitive to changes in the trait, reducing
sensitivity to variation (Brantley et al., 2011; Gamon et al., 1995; Sellers, 1985; Wang et al., 2005). In contrast, traits that
475   primarily affect specific spectral regions, such as Chl and Car, which mainly influence the visible spectrum, may not be fully
captured by the distance-based approach, potentially leading to an underestimation of uncertainty.

4.2 Landscape-Scale Uncertainty in OOD data

We further tested the performance of these methods on the landscape scale with two scenes from distinct sensors, each
480   containing a variety of scene components that are not typically in the training data. This served as a proof of concept to
assess models' behavior under extreme OOD conditions, as it is hard to visually validate the predictions with no reference
data. In such cases, a higher range of uncertainty should indicate regions where the model is not confident.

4.2.1 Comparison with other methods

485 Despite being trained exclusively on vegetation samples, the Dis_Un method demonstrated robust performance in detecting shifts in the distribution of different scene components - even if they are not vegetation. The Dis_UN performance was comparable to that of the Ens_UN method and superior to the MCdrop_UN approach, as evidenced by the JM distance metric (Fig 6 and 7). Both the Dis_UN method and Ens_UN showed similar trends in uncertainty estimation: regions with high and low uncertainty values were consistently identified by both methods. However, the Dis_UN method exhibited a

490 broader range of uncertainty, allowing for finer differentiation across different regions. This comparability with Ens_UN is expected, given that the same trained models were used to develop both methods. However, when examining the spatial uncertainty maps, the Dis_UN method produced more homogeneous boundaries within the scene components, highlighting its ability to provide more consistent spatial representations of uncertainty (Figs 4, 5, 6, 7). Results from the Kolmogorov-Smirnov (KS) test further demonstrated that the Dis_UN method produced distinct uncertainty distributions for vegetated

495 and non-vegetated pixels, with non-vegetated areas consistently showing higher residuals across all traits (Figs. 4, 5).

In contrast, the MCdrop_UN method consistently demonstrated the weakest performance, raising concerns about its reliability in these contexts, particularly when assessing model uncertainty. One key issue is that low standard deviation values may create a false sense of confidence in the model's predictions, suggesting better trait model performance than what is actually the case. This can be misleading, as the narrow range of uncertainty estimates does not necessarily reflect

500 the true error in the model's outputs. Such behavior has been observed in previous studies (e.g., Pullanagari et al. 2021, Padarian et al. 2022, García-Soria et al. 2024), where dropout-based uncertainty appeared overly optimistic in comparison to other uncertainty assessment methods. To avoid potential misinterpretations, it is crucial to consider alternative metrics and methods when evaluating uncertainty estimation approaches. For instance, relying solely on standard deviation values or similar variance-based metrics may overlook important aspects of model performance, such as the method's ability to

505 capture OOD uncertainty or account for heterogeneity in complex datasets.

Beyond enhancing uncertainty prediction performances, the proposed distance-based uncertainty estimation method provides substantial computational advantages over variance-based approaches. Unlike variance-based methods that require multiple forward passes to compute prediction variance, the distance-based approach allows for straightforward application once the uncertainty model is trained. This eliminates the need for repeated inference runs, making it significantly more

510 computationally efficient. Such efficiency is particularly valuable for large-scale remote sensing applications, where fast and scalable uncertainty estimation is crucial.

4.2.2 Uncertainty Patterns Across scene components and Spatial Resolutions

For the EnMAP scene, with 30 m spatial resolution, the uncertainty maps showed a variation in uncertainty among traits.

515 This is expected because the different traits depend on distinct spectral regions, which are affected differently by various scene components (e.g., water, urban areas, or vegetation). Higher uncertainty was particularly evident in non-vegetative land cover types such as water, cloud and cloud-shadow regions, which are clearly OOD relative to the model's primary

focus on vegetation. These areas lack spectral similarity to vegetation and therefore result in increased uncertainty in the model's predictions. In contrast, urban areas exhibited lower uncertainty, a pattern that can be explained by the mixed

520   component in such areas. Urban areas often contain green spaces, like trees and meadow patches. As a result, these mixed pixels are closer to vegetation data of the training set and do not show as strong uncertainties as pure non-vegetative classes like water. These results highlight that the method works as expected independently from the land cover types and scene components, so that with gradual dissimilarity from vegetation spectra, the uncertainty increases. As shown here at the example of the 30m EnMap data, such an uncertainty quantification is particularly important to evaluate the robustness of a

525   prediction in complex scenes, where more than one land cover type can be present per pixel and the resolution of the sensor and existing land cover products are not detailed enough to explicitly resolve the scene component.

While most of the traits showed a similar spatial pattern in the predicted uncertainties (Fig. 4 and 5), also when compared to the range of uncertainty values of training data samples (Fig. S7 and S10), LAI was distinguishingly different. Traits, such as LMA, EWT and N, exhibit lower uncertainty in areas with dense canopies, where a strong leaf signal is present. This

530   contrasts with LAI, which shows greater uncertainty in dense vegetation, likely due to saturation effects—where increases in leaf area are no longer detectable by the sensor. This saturation issue is common for LAI that have limited sensitivity in dense vegetation conditions (Asner et al., 2003; Mutanga et al., 2023). A particularly unique behavior observed in LAI uncertainty predictions, where higher uncertainties were detected in dense vegetation areas, while lower uncertainties were observed in OOD pixels, such as water, shadow, and urban regions but with low variations. This pattern diverged from the

535   behavior of other traits, where uncertainties were typically higher in OOD regions due to substantial deviations between the predicted trait values and training data distributions of the multi-trait model (Fig. S8 and S11).

For the EnMAP scene, we identified pure vegetated pixels representing different vegetation types, including crops, tree cover, and grassland. As discussed in Section 4.1, grassland pixels exhibited the lowest uncertainty with minimal variation, likely due to their simpler spectral properties. Crops showed the highest uncertainty values but with lower variation, while

540   tree cover and shrubland displayed high variability in predicted uncertainty, reflecting their greater spectral and structural complexity (Fig. S13). We observed a similar pattern for the 1m resolution NEON data. Uncertainty in the vegetated areas (forest) exhibited greater variability (bimodal distribution, Fig. 5) in the NEON scene compared to vegetated areas in the EnMAP scene. This suggests that uncertainty in forested regions may be more sensitive to fine-scale shadows and canopy structural complexity, resulting in a more complex spectral response. These small-scale confounding factors, such as those

545   from canopy gaps and canopy structures, substantially affect the spectral response (Nagendra and Rocchini, 2008).

4.3 Challenges in training uncertainty models

Training uncertainty models for trait prediction in remote sensing is subject to substantial challenges due to the sparse and non-uniform distribution of available trait data. This lack of comprehensive data coverage is particularly problematic at the

550   low and high ends of the trait distribution. Very low trait values often are associated with weak signals while high trait values can lead to saturation effects, both resulting in high uncertainty estimation, when using Dis_UN. This data sparsity

not only limits the model's ability to make robust trait predictions but also prevents the training of models to robustly estimate uncertainty across the full trait range. Moving forward, it is crucial to collect more data, particularly from the tails of the trait distributions (e.g., very high or low values). This means not only gathering data from plants at the peak of their

555   growing season, when they exhibit high vitality, but also from senescent or stressed plants, which are typically underrepresented in current datasets (Schiefer et al. 2021, Brown et al., 2020). Such efforts underscore the importance of data sharing within the scientific community to improve the robustness and reliability of uncertainty models (Cherif et al. 2023).

560   **4.4 Challenges in comparing and interpreting the uncertainty of state-of-the-art methods**

Comparing and interpreting the uncertainty estimates produced by different state-of-the-art methods presents challenges, particularly due to the underlying assumptions of each approach. Traditional methods, such as Ens_UN techniques and MCdrop_UN, often assume Gaussian uncertainty, implying that errors are symmetrically distributed around the mean (Hu et al., 2022; Klotz et al., 2022). However, this assumption does not hold true for many plant trait distributions, which are

565   inherently skewed and variable due to ecological and physiological factors across diverse vegetation types—including forests, grasslands, and crops. Models that cannot account for this asymmetry will produce biased or inaccurate uncertainty estimates, as they assume that the data's spread around the mean is similar on both sides. For instance, Klotz et al. (2022) emphasize the importance of accounting for asymmetric distributions in natural data, noting how uncertainty estimates can be improved by modeling heavy tails and skewed data. While their focus was on hydrological modeling, similar asymmetries

570   are present in plant trait values, making their insights applicable to our context. When plant trait distributions are skewed, their corresponding uncertainty estimates should reflect this asymmetry. Enforcing a symmetric error structure leads to systematic misrepresentation, typically underestimating uncertainty in the long tail while overestimating elsewhere. This miscalibration results in predictive intervals that do not align with observed variability. In contrast, a well-calibrated approach that accounts for asymmetric error structures can provide more reliable and accurate uncertainty estimates,

575   ensuring proper coverage across the full trait range, regardless of whether the underlying distribution is Gaussian.

Moreover, Janet et al. (2019) reveal that traditional uncertainty estimation methods such as MCdrop_UN and Ens_UN often produce overly confident predictions in OOD regions. In our study, MCdrop_UN and Ens_UN methods exhibited similar tendencies, particularly when applied to OOD samples with unfamiliar spectral characteristics due to different sensor properties and scene elements like water and clouds. This overconfidence in OOD regions is problematic, as it can lead to a

580   false sense of reliability in model predictions where the model is actually less certain.

Variance-based approaches have notable limitations in uncertainty estimation. While they provide a measure of dispersion, their uncertainties do not always scale appropriately with the actual errors, making direct interpretation and practical application challenging (Fig. 3). The Ens_UN method, in particular, has been observed to underestimate uncertainty, providing an optimistic assessment of model performance (Janet et al., 2019; Meyer and Pebesma, 2021). This can be

585   misleading, especially in cases where the predictor is inherently biased, but the variations within the Ens_UN are small,

giving a false and often optimistic impression of reliability. Additionally, uncertainty is trait-specific, influenced by the intrinsic nature of the trait being predicted. Thus, interpreting uncertainty in these models requires careful consideration of both the method used and the specific trait characteristics, to avoid misinterpretation and ensure the reliability of predictions.

590 Unlike conventional methods, which largely reflect the uncertainty inherent in the training data, the distance-based approach adapts to new data by comparing it with the training set, offering a more comprehensive and flexible assessment of uncertainty.

4.5 Outlook: Uncertainty in the Context of Global Trait Mapping

Estimating uncertainty from remote sensing-based machine learning algorithms remains challenging, as current methods

595 struggle to capture the full complexity and diversity of real-world data and datasets are often limited in representativeness and quantity. Despite these issues, the distance-based method shows promise due to its increased interpretability compared to more complex probabilistic approaches. The distance-based method offers a clearer view of where and why high uncertainty arises, particularly in areas substantially different from the training data. By measuring the distance from known data, it intuitively identifies OOD regions, providing insights into the model's reliability under shifting conditions. Looking forward,

600 further refinement of the distance-based method could involve testing on more diverse datasets and exploring hybrid approaches that combine it with complementary probabilistic techniques.

5 Conclusion

Accurate methods for predicting uncertainty from machine learning models are lacking for vegetation monitoring. As an

605 example of trait prediction from hyperspectral data, this study demonstrates that traditional uncertainty quantification methods, such as ensemble and dropout Bayesian approaches, often struggle to adapt to unseen (OOD) data, resulting in overconfident or misleading uncertainty estimates. The presented distance-based method, however, offers improved adaptability across land cover types. Our results highlight the importance of incorporating diverse datasets to mitigate distributional biases. Furthermore, the proposed uncertainty method was successfully tested across two scenes acquired by

610 different sensors, with varying resolutions, across different biomes and land cover types, demonstrating its robustness across heterogeneous conditions. Accordingly, such an approach could be used for prediction of uncertainty in large-scale assessments, where OOD data is prevalent and reliable uncertainty estimation is crucial.

Data and code availability

615 The code for this study is available at: https://github.com/echerif18/Multi_trait_Uncertainty/

Declaration of Competing Interest

The authors declare that they have no known competing financial interests or personal relationships.

620 **Author Contributions**

EC contributed to the conceptualization, methodology, formal analysis, data curation, visualization, and writing of the original draft. HF and TK contributed to conceptualization, data curation, supervision, and writing of the original draft. LK, KB, PD, ME, TH, EL and BL provided data and contributed to writing, review and editing.

625 **Acknowledgements**

We thank all data owners for sharing the data either by request or through the public Ecological Spectral Information System (EcoSIS), Data Publisher for Earth & Environmental Science (PANGEA) and DRYAD platforms. EC and HF acknowledge the financial support by the Federal Ministry of Education and Research of Germany and by the Sächsische Staatsministerium für Wissenschaft Kultur und Tourismus in the program Center of Excellence for AI-research "Center for 630 Scalable Data Analytics and Artificial Intelligence Dresden/Leipzig", project identification number: ScaDS.AI. HF and TK acknowledge support for this work from the Federal Ministry for Economic Affairs and Climate Action (BMWK) and the German Aerospace Center (DLR) through the project AIResVeg (grant 50EE2203A). LK acknowledges that this activity was partly carried out under the Living Planet Fellowship, a program funded by the European Space Agency. The view expressed in this publication can in no way be taken to reflect the official opinion of the European Space Agency. This 635 study has been undertaken using data from "Fiducial Reference Measurements for Vegetation" (FRM4VEG), which was funded by the European Commission and managed by the European Space Agency under the Copernicus program, and "Fiducial Reference Measurements for Vegetation—Phase 2" (FRM4VEG—Phase 2), which was funded by the European Space Agency. This work was supported in part by the European Space Agency and European Commission through the Sentinel-3 Mission Performance Centre. This work was supported by MetEOC-4. The project 19ENV07 MetEOC-4 has 640 received funding from the EMPIR program co-financed by the Participating States and from the European Union's Horizon 2020 research and innovation program. Support for PD is from his faculty start-up package provided by Colorado State University.

References:

645 Abdar, M., and others: A review of uncertainty quantification in deep learning: Techniques, applications, and challenges, Inf. Fusion, 76, 243–297, 2021.

Asner, G. P.: Biophysical and biochemical sources of variability in canopy reflectance, Remote Sens. Environ., 64, 234–253, 1998.

Asner, G. P., Scurlock, J. M. O., and Hicke, J. A.: Global synthesis of leaf area index observations: implications for 650 ecological and remote sensing studies, Glob. Ecol. Biogeogr., 12, 191–205, 2003.

Asner, G. P. and Martin, R. E.: Spectranomics: Emerging science and conservation opportunities at the interface of biodiversity and remote sensing, Glob. Ecol. Conserv., 8, 212–219, 2016.

Briottet, X., Bajjouk, T., Chami, M., Delacourt, C., Feret, J.-B., Jacquemoud, S., Minghelli, A., Sheeren, D., Weber, C., Fabre, S., and others: BIODIVERSITY–A new space mission to monitor Earth ecosystems at fine scale, Rev. Fr. Photogramm. Télédétection, 224, 33–58, 2022.

Brantley, S. T., Zinnert, J. C., and Young, D. R.: Application of hyperspectral vegetation indices to detect variations in high leaf area index temperate shrub thicket canopies, Remote Sens. Environ., 115, 514–523, 2011.

Brodrick, P. G., Pavlick, R., Bernas, M., Chapman, J. W., Eckert, R., Helmlinger, M., Hess-Flores, M., Rios, L. M., Schneider, F. D., Smyth, M. M., Eastwood, M., Green, R. O., Thompson, D. R., Chadwick, K. D., and Schimel, D. S.: SHIFT: AVIRIS-NG L2A Unrectified Surface Reflectance Version 1, ORNL DAAC, Oak Ridge, Tennessee, USA, 2023.

Brown, L. A., Dash, J., Lidón, A. L., Lopez-Baeza, E., and Dransfeld, S.: Synergetic exploitation of the Sentinel-2 missions for validating the Sentinel-3 Ocean and Land Color Instrument terrestrial chlorophyll index over a vineyard dominated Mediterranean environment, IEEE J. Sel. Top. Appl. Earth Obs. Remote Sens., 12, 2244–2251, 2019.

Brown, L. A., Meier, C., Morris, H., Pastor-Guzman, J., Bai, G., Lerebourg, C., Gobron, N., Lanconelli, C., Clerici, M., and Dash, J.: Evaluation of global leaf area index and fraction of absorbed photosynthetically active radiation products over North America using Copernicus Ground Based Observations for Validation data, Remote Sens. Environ., 247, 111935, 2020.

Brown, L. A., Camacho, F., García-Santos, V., Origo, N., Fuster, B., Morris, H., Pastor-Guzman, J., Sánchez-Zapero, J., Morrone, R., Ryder, J., and others: Fiducial Reference Measurements for Vegetation Bio-Geophysical Variables: An End-to-End Uncertainty Evaluation Framework, Remote Sens. (Basel), 13, 3194, 2021a.

Brown, L. A., Fernandes, R., Djamai, N., Meier, C., Gobron, N., Morris, H., Canisius, F., Bai, G., Lerebourg, C., Lanconelli, C., and others: Validation of baseline and modified Sentinel-2 Level 2 Prototype Processor leaf area index retrievals over the United States, ISPRS J. Photogramm. Remote Sens., 175, 71–87, 2021b.

Brown, L. A., Morris, H., MacLachlan, A., D'Adamo, F., Adams, J., Lopez-Baeza, E., Albero, E., Martínez, B., Sánchez-Ruiz, S., Campos-Taberner, M., and others: Hyperspectral leaf area index and chlorophyll retrieval over forest and row-structured vineyard canopies, Remote Sens. (Basel), 16, 2066, 2024.

Burnett, A. C., Serbin, S. P., and Rogers, A.: Source-sink imbalance detected with leaf- and canopy-level spectroscopy in a field-grown crop, Plant Cell Environ., 44, 2466–2479, 2021.

Chadwick, K. D., Queally, N., Zheng, T., Cryer, J., Vanden Heuvel, C., Villanueva-Weeks, C., Ade, C., Anderegg, L., Angel, Y., Baker, B., and others: SHIFT: Photosynthetic and Leaf Traits, Santa Barbara County, 2022, ORNL DAAC, Oak Ridge, Tennessee, USA, 2023.

Camia, A., Gliottone, I., Dowell, M., Vancutsem, C., Bertoglio, C.: Earth Observation for Biodiversity, European Commission, Ispra (Italy), 2024.

Camps-Valls, G., Campos-Taberner, M., Moreno-Martínez, Á., Walther, S., Duveiller, G., Cescatti, A., Mahecha, M. D., Muñoz-Marí, J., García-Haro, F. J., Guanter, L., and others: A unified vegetation index for quantifying the terrestrial biosphere, Sci. Adv., 7, eabc7447, 2021.

Cavender-Bares, J., Gamon, J. A., Hobbie, S. E., Madritch, M. D., Meireles, J. E., Schweiger, A. K., and Townsend, P. A.: Harnessing plant spectra to integrate the biodiversity sciences across biological and spatial scales, Am. J. Bot., 104, 966–969, 2017.

690 Cavender-Bares, J., Gamon, J. A., and Townsend, P. A.: Remote sensing of plant biodiversity, Springer Nature, 2020.

Cawse-Nicholson, K., Townsend, P. A., Schimel, D., Assiri, A. M., Blake, P. L., Buongiorno, M. F., Campbell, P., Carmon, N., Casey, K. A., Correa-Pabón, R. E., and others: NASA's surface biology and geology designated observable: A perspective on surface imaging algorithms, Remote Sens. Environ., 257, 112349, 2021.

Cerasoli, S., Campagnolo, M., Faria, J., Nogueira, C., and Caldeira, M. C.: On estimating the gross primary productivity of
695 Mediterranean grasslands under different fertilization regimes using vegetation indices and hyperspectral reflectance, Biogeosciences, 15, 5455–5471, 2018.

Chabrillat, S., Foerster, S., Segl, K., Beamish, A., Brell, M., Asadzadeh, S., Milewski, R., Ward, K. J., Brosinsky, A., Koch, K., and others: The EnMAP spaceborne imaging spectroscopy mission: Initial scientific results two years after launch, Remote Sens. Environ., 114379, 2024.

700 Cherif, E., Feilhauer, H., Berger, K., Dao, P. D., Ewald, M., Hank, T. B., He, Y., Kovach, K. R., Lu, B., Townsend, P. A., and others: From spectra to plant functional traits: Transferable multi-trait models from heterogeneous and sparse data, Remote Sens. Environ., 292, 113580, 2023.

Chernetskiy, M., Gómez-Dans, J., Gobron, N., Morgan, O., Lewis, P., Truckenbrodt, S., and Schmullius, C.: Estimation of FAPAR over croplands using MISR data and the earth observation land data assimilation system (EO-LDAS), Remote Sens.
705 (Basel), 9, 656, 2017.

Chlus, A., Kruger, E. L., and Townsend, P. A.: Mapping three-dimensional variation in leaf mass per area with imaging spectroscopy and LiDAR in a temperate broadleaf forest, Remote Sens. Environ., 250, 112043, 2020.

Cogliati, S., Sarti, F., Chiarantini, L., Cosi, M., Lorusso, R., Lopinto, E., Miglietta, F., Genesio, L., Guanter, L., Damm, A., and others: The PRISMA imaging spectroscopy mission: Overview and first performance analysis, Remote Sens. Environ.,
710 262, 112499, 2021.

Dao, P. D., Axiotis, A., and He, Y.: Mapping native and invasive grassland species and characterizing topography-driven species dynamics using high spatial resolution hyperspectral imagery, Int. J. Appl. Earth Obs. Geoinf., 104, 102542, 2021.

De Los Reyes, R., Langheinrich, M., and Bachmann, M.: EnMAP ground segment-level 2A Processor (atmospheric correction over land) ATBD, EN-PCV-TN-6007, 2, 2023.

715 Douze, M., and others: The FAISS library, arXiv preprint, arXiv:2401.08281, 2024.

Deng, Z., Zhou, F., Chen, J., Wu, G., and Zhu, J.: Deep ensemble as a Gaussian process approximate posterior, arXiv preprint arXiv:2205.00163, 2022.

Efron, B. and Tibshirani, R. J.: An introduction to the bootstrap, Vol. 57, CRC Press, 1993.

Ewald, M., Skowronek, S., Aerts, R., Dolos, K., Lenoir, J., and others: Analyzing remotely sensed structural and chemical
720 canopy traits of a forest invaded by Prunus serotina over multiple spatial scales, Biol. Invasions, 20, 2257–2271, 2018.

Ewald, M., Skowronek, S., Aerts, R., Lenoir, J., Feilhauer, H., and others: Assessing the impact of an invasive bryophyte on plant species richness using high-resolution imaging spectroscopy, Ecol. Indic., 110, 105882, 2020.

Feilhauer, H., Zlinszky, A., Kania, A., Foody, G. M., Doktor, D., Lausch, A., and Schmidtlein, S.: Let your maps be fuzzy!—Class probabilities and floristic gradients as alternatives to crisp mapping for remote sensing of vegetation, Remote

725 Sens. Ecol. Conserv., 7, 292–305, 2021.

Feilhauer, H., and others: Brightness-normalized partial least squares regression for hyperspectral data, J. Quant. Spectrosc. Radiat. Transf., 111, 1947–1957, 2010.

Funk, J. L., Larson, J. E., Ames, G. M., Butterfield, B. J., Cavender-Bares, J., Firn, J., Laughlin, D. C., Sutton-Grier, A. E., Williams, L., and Wright, J.: Revisiting the H oly G rail: using plant functional traits to understand ecological processes,

730 Biological Reviews, 92, 1156–1173, 2017.

Gal, Y. and others: Uncertainty in deep learning, 2016.

Gal, Y. and Ghahramani, Z.: Dropout as a Bayesian approximation: Representing model uncertainty in deep learning, in: International Conference on Machine Learning, 1050–1059, 2016.

García-Soria, J. L., Morata, M., Berger, K., Pascual-Venteo, A. B., Rivera-Caicedo, J. P., and Verrelst, J.: Evaluating

735 epistemic uncertainty estimation strategies in vegetation trait retrieval using hybrid models and imaging spectroscopy data, Remote Sens. Environ., 310, 114228, 2024.

Gamon, J. A., Field, C. B., Goulden, M. L., Griffin, K. L., Hartley, A. E., Joel, G., Penuelas, J., and Valentini, R.: Relationships between NDVI, canopy structure, and photosynthesis in three Californian vegetation types, Ecol. Appl., 5, 28–41, 1995.

740 Garg, A., Patil, A., Sarkar, M., Moorthi, S. M., and Dhar, D.: Advancements in data processing and calibration for the Hyperspectral Imaging Satellite (HySIS), arXiv preprint arXiv:2411.08917, 2024.

Ge, X., Ding, J., Teng, D., Xie, B., Zhang, X., Wang, J., Han, L., Bao, Q., and Wang, J.: Exploring the capability of Gaofen-5 hyperspectral data for assessing soil salinity risks, Int. J. Appl. Earth Obs. Geoinf., 112, 102969, 2022.

Gorroño, J., Fomferra, N., Peters, M., Gascon, F., Underwood, C. I., Fox, N. P., Kirches, G., and Brockmann, C.: A

745 radiometric uncertainty tool for the Sentinel-2 mission, Remote Sens. (Basel), 9, 178, 2017.

Gorroño, J., Hunt, S., Scanlon, T., Banks, A., Fox, N., Woolliams, E., Underwood, C., Gascon, F., Peters, M., Fomferra, N., and others: Providing uncertainty estimates of the Sentinel-2 top-of-atmosphere measurements for radiometric validation activities, Eur. J. Remote Sens., 51, 650–666, 2018.

Goryl, P., Fox, N., Donlon, C., and Castracane, P.: Fiducial reference measurements (FRMs): What are they?, Remote Sens.

750 (Basel), 15, 5017, 2023.

Graf, L. V., Gorroño, J., Hueni, A., Walter, A., and Aasen, H.: Propagating Sentinel-2 top-of-atmosphere radiometric uncertainty into land surface phenology metrics using a Monte Carlo framework, IEEE J. Sel. Top. Appl. Earth Obs. Remote Sens., 16, 8632–8654, 2023.

Gravel, A., Laliberté, E., and Kalacska, M.: Foliar functional trait mapping of a mixed temperate forest using imaging
755   spectroscopy, Federated Research Data Repository, 2024.

Hank, T. B., Berger, K., Bach, H., Clevers, J. G. P. W., Gitelson, A., Zarco-Tejada, P., and Mauser, W.: Spaceborne imaging
spectroscopy for sustainable agriculture: Contributions and challenges, Surv. Geophys., 40, 515–551, 2019.

Hank, T., Locherer, M., Richter, K., Mauser, W., Consortium, E., and others: Neusling (Landau ad Isar) 2012—a
multitemporal and multisensoral agricultural EnMAP Preparatory Flight Campaign, 2016.

760   Hank, T., Richter, K., Mauser, W., Consortium, E., and others: Neusling (Landau ad Isar) 2009—an agricultural EnMAP
Preparatory Flight Campaign using the HyMap instrument, 2015.

Herrmann, I., Pimstein, A., Karnieli, A., Cohen, Y., Alchanatis, V., and Bonfil, D. J.: LAI assessment of wheat and potato
crops by VENμS and Sentinel-2 bands, Remote Sens. Environ., 115, 2141–2151, 2011.

Houborg, R., Fisher, J. B., and Skidmore, A. K.: Advances in remote sensing of vegetation function and traits, Int. J. Appl.
765   Earth Obs. Geoinf., 2015.

Hu, Y., Musielewicz, J., Ulissi, Z. W., and Medford, A. J.: Robust and scalable uncertainty estimation with conformal
prediction for machine-learned interatomic potentials, Mach. Learn. Sci. Technol., 3, 45028, 2022.

Jacquemoud, S. and Ustin, S.: Leaf optical properties, Cambridge University Press, 2019.

Janet, J. P., Duan, C., Yang, T., Nandy, A., and Kulik, H. J.: A quantitative uncertainty metric controls error in neural
770   network-driven chemical discovery, Chem. Sci., 10, 7913–7922, 2019.

Joint Committee for Guides in Metrology (JCGM): Evaluation of measurement data—Guide to the expression of uncertainty
in measurement, Int. Organ. Stand. Geneva ISBN, 50, 134, 2008..

Jetz, W., Cavender-Bares, J., Pavlick, R., Schimel, D., Davis, F. W., Asner, G. P., Guralnick, R., Kattge, J., Latimer, A. M.,
and Moorcroft, P.: Monitoring plant functional diversity from space, Nat. Plants, 2, 1–5, 2016.

775   Kampe, T. U., Johnson, B. R., Kuester, M. A., and Keller, M.: NEON: The first continental-scale ecological observatory
with airborne remote sensing of vegetation canopy biochemistry and structure, J. Appl. Remote Sens., 4, 43510, 2010.

Kattenborn, T., Fassnacht, F. E., and Schmidtlein, S.: Differentiating plant functional types using reflectance: Which traits
make the difference?, Remote Sens. Ecol. Conserv., 5, 5–19, 2019.

Kattenborn, T., Schiefer, F., Frey, J., Feilhauer, H., Mahecha, M. D., and Dormann, C. F.: Spatially autocorrelated training
780   and validation samples inflate performance assessment of convolutional neural networks, ISPRS Open J. Photogramm.
Remote Sens., 5, 100018, 2022.

Khatami, R., Mountrakis, G., and Stehman, S. V.: Mapping per-pixel predicted accuracy of classified remote sensing images,
Remote Sens. Environ., 191, 156–167, 2017.

Kissling, W. D., Walls, R., Bowser, A., Jones, M. O., Kattge, J., Agosti, D., Amengual, J., Basset, A., Van Bodegom, P. M.,
785   Cornelissen, J. H. C., and others: Towards global data products of Essential Biodiversity Variables on species traits, Nat.
Ecol. Evol., 2, 1531–1540, 2018.

Klotz, D., Kratzert, F., Gauch, M., Keefe Sampson, A., Brandstetter, J., Klambauer, G., Hochreiter, S., and Nearing, G.: Uncertainty estimation with deep learning for rainfall–runoff modeling, Hydrol. Earth Syst. Sci., 26, 1673–1693, 2022.

Koenker, R., and Hallock, K. F.: Quantile regression, J. Econ. Perspect., 15, 143–156, 2001.

790 Kruse, F. A., Lefkoff, A. B., Boardman, J. W., Heidebrecht, K. B., Shapiro, A. T., Barloon, P. J., and Goetz, A. F. H.: The spectral image processing system (SIPS)—interactive visualization and analysis of imaging spectrometer data, Remote Sens. Environ., 44, 145–163, 1993.

Lakshminarayanan, B., Pritzel, A., and Blundell, C.: Simple and scalable predictive uncertainty estimation using deep ensembles, Adv. Neural Inf. Process. Syst., 30, 2017.

795 Lang, N., Kalischek, N., Armston, J., Schindler, K., Dubayah, R., and Wegner, J. D.: Global canopy height regression and uncertainty estimation from GEDI LIDAR waveforms with deep ensembles, Remote Sens. Environ., 268, 112760, 2022.

Lavorel, S. and Garnier, É.: Predicting changes in community composition and ecosystem functioning from plant traits: revisiting the Holy Grail, Funct Ecol, 16, 545–556, 2002.

Levi, D., Gispan, L., Giladi, N., and Fetaya, E.: Evaluating and calibrating uncertainty prediction in regression tasks, 800 Sensors, 22, 2022.

Lewis, P., Gómez-Dans, J., Kaminski, T., Settle, J., Quaife, T., Gobron, N., Styles, J., and Berger, M.: An earth observation land data assimilation system (EO-LDAS), Remote Sens. Environ., 120, 219–235, 2012.

Linnenbrink, J., Milà, C., Ludwig, M., and Meyer, H.: kNNDM CV: k-fold nearest-neighbour distance matching cross-validation for map accuracy estimation, Geosci. Model Dev., 17, 5897–5912, 2024.

805 Liu, J. Z., and others: A simple approach to improve single-model deep uncertainty via distance-awareness, J. Mach. Learn. Res., 24, 42, 1–63, 2023.

Martínez-Ferrer, L., Moreno-Martínez, Á., Campos-Taberner, M., García-Haro, F. J., Muñoz-Marí, J., Running, S. W., Kimball, J., Clinton, N., and Camps-Valls, G.: Quantifying uncertainty in high-resolution biophysical variable retrieval with machine learning, Remote Sens. Environ., 280, 113199, 2022.

810 Mathieu, P.-P. and O'Neill, A.: Data assimilation: From photon counts to Earth System forecasts, Remote Sens. Environ., 112, 1258–1267, 2008.

Meyer, H. and Pebesma, E.: Predicting into unknown space? Estimating the area of applicability of spatial prediction models, Methods Ecol. Evol., 12, 1620–1633, 2021.

Mutanga, O., Masenyama, A., and Sibanda, M.: Spectral saturation in the remote sensing of high-density vegetation traits: A 815 systematic review of progress, challenges, and prospects, ISPRS J. Photogramm. Remote Sens., 198, 297–309, 2023.

Nagendra, H. and Rocchini, D.: High-resolution satellite imagery for tropical biodiversity studies: the devil is in the detail, Biodivers. Conserv., 17, 3431–3442, 2008.

Nieke, J., Despoisse, L., Gabriele, A., Weber, H., Strese, H., Ghasemi, N., Gascon, F., Alonso, K., Boccia, V., Tsonevska, B., Choukroun, P., Ottavianelli, G., and Celesti, M.: The Copernicus Hyperspectral Imaging Mission for the Environment

820   (CHIME): an overview of its mission, system, and planning status, in: Sensors, Systems, and Next-Generation Satellites XXVII, 1272909, 2023.

Ollinger, S. V.: Sources of variability in canopy reflectance and the convergent properties of plants, New Phytol., 189, 375–394, 2011.

Padarian, J., Minasny, B., & McBratney, A. B. (2022). Assessing the uncertainty of deep learning soil spectral models using
825   Monte Carlo dropout. *Geoderma, 425*, 116063.

Papacharalampous, G., and others: Uncertainty estimation of machine learning spatial precipitation predictions from satellite data, Mach. Learn. Sci. Technol., 5, 035044, 2024.

Ploton, P., Mortier, F., Réjou-Méchain, M., Barbier, N., Picard, N., Rossi, V., Dormann, C., Cornu, G., Viennois, G., Bayol, N., and others: Spatial validation reveals poor predictive performance of large-scale ecological mapping models, Nat.
830   Commun., 11, 4540, 2020.

Pottier, J., Malenovský, Z., Psomas, A., Homolová, L., Schaepman, M. E., and others: Modelling plant species distribution in alpine grasslands using airborne imaging spectroscopy, Biol. Lett., 10, 20140347, 2014.

Pullanagari, R. R., Dehghan-Shoar, M., Yule, I. J., and Bhatia, N.: Field spectroscopy of canopy nitrogen concentration in temperate grasslands using a convolutional neural network, Remote Sens. Environ., 257, 112353, 2021.

835   Reich PB (2014) The world-wide 'fast–slow' plant economics spectrum: a traits manifesto. J Ecol 102:275–301

Richards, J. A., Richards, J. A., and others: Remote sensing digital image analysis, Springer, 2022.

Rogers, A., Serbin, S., and Ely, K.: Leaf mass area, leaf carbon and nitrogen content, Kougarok Road and Teller Road, Seward Peninsula, Alaska, 2016, 2021.

Sakschewski, B., von Bloh, W., Boit, A., Rammig, A., Kattge, J., Poorter, L., Peñuelas, J., and Thonicke, K.: Leaf and stem
840   economics spectra drive diversity of functional plant traits in a dynamic global vegetation model, Glob. Chang. Biol., 21, 2711–2725, 2015.

Savitzky, A. and Golay, M. J. E.: Smoothing and differentiation of data by simplified least squares procedures, Anal. Chem., 36, 1627–1639, 1964.

Scalia, G., Grambow, C. A., Pernici, B., Li, Y.-P., and Green, W. H.: Evaluating scalable uncertainty estimation methods for
845   deep learning-based molecular property prediction, J. Chem. Inf. Model., 60, 2697–2717, 2020.

Schiefer, F., Schmidtlein, S., and Kattenborn, T.: The retrieval of plant functional traits from canopy spectra through RTM-inversions and statistical models are both critically affected by plant phenology, Ecol. Indic., 121, 107062, 2021.

Sellers, P. J.: Canopy reflectance, photosynthesis, and transpiration, Int. J. Remote Sens., 6, 1335–1372, 1985.

Serbin, S. P., Wu, J., Ely, K. S., Kruger, E. L., Townsend, P. A., Meng, R., Wolfe, B. T., Chlus, A., Wang, Z., and Rogers,
850   A.: From the Arctic to the tropics: multibiome prediction of leaf mass per area using leaf reflectance, New Phytol., 224, 1557–1568, 2019.

Serbin, S. P., and Townsend, P. A.: Scaling functional traits from leaves to canopies, in: Remote Sensing of Plant Biodiversity, pp. 43–82, 2020

Silvan-Cardenas, J. L. and Wang, L.: Sub-pixel confusion–uncertainty matrix for assessing soft classifications, Remote Sens.
855   Environ., 112, 1081–1195, 2008.

Singh, A., Serbin, S. P., McNeil, B. E., Kingdon, C. C., and Townsend, P. A.: Imaging spectroscopy algorithms for mapping canopy foliar chemical and morphological traits and their uncertainties, Ecol. Appl., 25, 2180–2197, 2015.

Ting, Z., Ye, Z., Singh, A., Desai, A. R., Krishnayya, N. S. R., Dave, M. G., and Townsend, P. A.: Plot-level traits and their corresponding image spectra from the Western Ghats of India, Ecological Spectral Information System (EcoSIS), 2023.

860   Van Cleemput, E., Roberts, D. A., Honnay, O., and Somers, B.: A novel procedure for measuring functional traits of herbaceous species through field spectroscopy, Methods Ecol. Evol., 10, 1332–1338, 2019.

Van Bodegom, P. M., Douma, J. C., and Verheijen, L. M.: A fully traits-based approach to modeling global vegetation distribution, Proc. Natl. Acad. Sci. USA, 111, 13733–13738, 2014.

Wacker, A. G. and Landgrebe, D. A.: Minimum distance classification in remote sensing, LARS Tech. Rep., 25, 1972.

865   Wang, D. R., Wolfrum, E. J., Virk, P., Ismail, A., Greenberg, A. J., and McCouch, S. R.: Robust phenotyping strategies for evaluation of stem non-structural carbohydrates (NSC) in rice, J. Exp. Bot., 67, 6125–6138, 2016.

Wang, Z., Townsend, P. A., Schweiger, A. K., Couture, J. J., Singh, A., Hobbie, S. E., and Cavender-Bares, J.: Mapping foliar functional traits and their uncertainties across three years in a grassland experiment, Remote Sens. Environ., 221, 405–416, 2019.

870   Wang, Z., Chlus, A., Geygan, R., Ye, Z., Zheng, T., Singh, A., and others: Foliar functional traits from imaging spectroscopy across biomes in eastern North America, New Phytol., 228, 494–511, 2020.

Wang, Q., Adiku, S., Tenhunen, J., and Granier, A.: On the relationship of NDVI with leaf area index in a deciduous forest site, Remote Sens. Environ., 94, 244–255, 2005.

Wocher, M., Berger, K., Danner, M., Mauser, W., and Hank, T.: Physically-based retrieval of canopy equivalent water
875   thickness using hyperspectral data, Remote Sens. (Basel), 10, 1924, 2018.

Widlowski, J.-L.: Conformity testing of satellite-derived quantitative surface variables, Environ. Sci. Policy, 51, 149–169, 2015.

Zheng, T., Ye, Z., Singh, A., Desai, A. R., Krishnayya, N. S. R., Dave, M. G., and Townsend, P. A.: Plot-level traits and their corresponding image spectra from the Western Ghats of India, Ecological Spectral Information System (EcoSIS), 2023.